JOINT TRANSPORTATION
RESEARCH PROGRAM
INDIANA DEPARTMENT OF TRANSPORTATION
AND PURDUE UNIVERSITY

Feasibility of 3D Scanning Technology for Bridge Inspection and Management

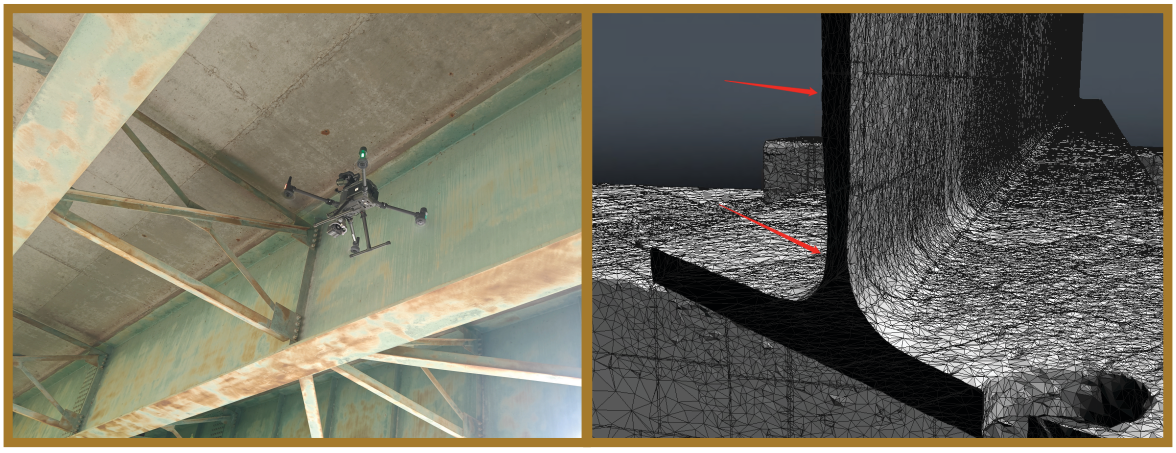

Kyubyung Kang, Jinwu Xiao, Jiashu Hu, Deven Surya
Chandan Kanakamedala, Jungil Seo, and Amit Varma

SPR-4731 • Report Number: FHWA/IN/JTRP-2025/16 • DOI: 10.5703/1288284317880

RECOMMENDED CITATION

Kang, K., Xiao, J., Hu, J., Kanakamedala, D. S. C., Seo, J., & Varma, A. (2025). *Feasibility of 3D scanning technology for bridge inspection and management* (Joint Transportation Research Program Publication No. FHWA/IN/JTRP-2025/16). West Lafayette, IN: Purdue University. https://doi.org/10.5703/1288284317880

AUTHORS

Kyubyung Kang, PhD
Assistant Professor
Bowen School of Construction
Purdue University
(765) 496-0796
kyukang@purdue.edu
Corresponding Author

Jinwu Xiao
Research Assistant
Bowen School of Construction
Purdue University

Jiashu Hu
Research Assistant
Bowen School of Construction
Purdue University

Deven Surya Chandan Kanakamedala
Purdue University

Jungil Seo, PhD
Research Scientist, Sr. Principal
Lyles School of Civil and Construction Engineering
Purdue University

Amit Varma, PhD
Karl H. Kettelhut Professor of Civil Engineering
Lyles School of Civil and Construction Engineering
Purdue University

JOINT TRANSPORTATION RESEARCH PROGRAM

The Joint Transportation Research Program serves as a vehicle for INDOT collaboration with higher education institutions and industry in Indiana to facilitate innovation that results in continuous improvement in the planning, design, construction, operation, management and economic efficiency of the Indiana transportation infrastructure. Learn more at engineering.purdue.edu/JTRP.

Published reports of the Joint Transportation Research Program are available at docs.lib.purdue.edu/jtrp/.

NOTICE

TECHNICAL REPORT DOCUMENTATION PAGE

1. Report No. FHWA/IN/JTRP-2025/16	**2. Government Accession No.**	**3. Recipient's Catalog No.**
4. Title and Subtitle Feasibility of 3D scanning technology for bridge inspection and management		**5. Report Date** June 3, 2025 **6. Performing Organization Code**
7. Author(s) Kyubyung Kang, PhD (https://orcid.org/0000-0001-7293-2171) Jinwu Xiao (https://orcid.org/0000-0002-9440-6719) Jiashu Hu Deven Surya Chandan Kanakamedala (https://orcid.org/0000-0002-8167-4183) Jungil Seo, PhD (https://orcid.org/0000-0003-0861-4261) Amit Varma, PhD (https://orcid.org/0000-0001-7153-4681)		**8. Performing Organization Report No.** FHWA/IN/JTRP-2025/16
9. Performing Organization Name and Address Joint Transportation Research Program Hall for Discovery and Learning Research (DLR), Suite 204 207 S. Martin Jischke Drive West Lafayette, IN 47907		**10. Work Unit No.** **11. Contract or Grant No.** SPR-4731
12. Sponsoring Agency Name and Address Indiana Department of Transportation (SPR) State Office Building 100 North Senate Avenue Indianapolis, IN 46204		**13. Type of Report and Period Covered** Final Report **14. Sponsoring Agency Code**

15. Supplementary Notes

Conducted in cooperation with the U.S. Department of Transportation, Federal Highway Administration.

16. Abstract

This report evaluates the feasibility of 3D scanning technologies, including LiDAR, terrestrial laser scanning (TLS), and UAV photogrammetry, for improving bridge inspection practices. The study identifies challenges in adopting these technologies, particularly for detecting corrosion, section loss, and deformation in steel girders and other critical structural components. A framework is developed to integrate 3D scanning data with defect detection and structural analysis tools, ensuring compatibility with existing bridge inspection and asset management systems. The report provides practical guidelines for optimizing scanning strategies, data processing workflows, and implementation procedures to support Indiana's bridge inspection practice. The proposed framework is designed to improve inspection accuracy, enhance efficiency, reduce field inspection time, and support data-driven decision-making for bridge maintenance and rehabilitation planning.

17. Key Words 3D scanning technology, bridge inspection, UAV photogrammetry, LiDAR, terrestrial laser scanning	**18. Distribution Statement** No restrictions. This document is available through the National Technical Information Service, Springfield, VA 22161.

19. Security Classif. (of this report) Unclassified	**20. Security Classif. (of this page)** Unclassified	**21. No. of Pages** 53, including appendices	**22. Price**

Form DOT F 1700.7 (8-72) Reproduction of completed page authorized

EXECUTIVE SUMMARY

Introduction

Ensuring the safety and longevity of Indiana's bridge infrastructure requires efficient and accurate inspection methods. Traditional techniques, such as visual assessments and nondestructive testing (NDT), provide valuable information but have limitations including subjectivity, accessibility challenges, and labor-intensive data collection. As infrastructure ages, there is an increasing need for advanced inspection technologies that can provide high-resolution, repeatable, and objective data for condition assessment and maintenance planning.

This study evaluates the feasibility of three-dimensional (3D) scanning technologies, such as terrestrial laser scanning (TLS), unmanned aerial vehicles (UAV) photogrammetry, close-range photogrammetry (CRP), and light detection and ranging (LiDAR), for bridge inspections, particularly for detecting corrosion, section loss, and deformation in steel bridge girders. A framework was developed to optimize scanning workflows, enhance data integration with structural analysis tools, and support decision-making. The report outlines key findings and presents practical recommendations for incorporating 3D scanning into Indiana's bridge inspection program.

Findings

The study confirmed the accuracy and effectiveness of 3D scanning technologies and identified key benefits and challenges:

- *Scanning Accuracy and Coverage*: TLS and UAV photogrammetry demonstrated high-resolution geometric detail capture for steel bridge components, including steel girders, deck soffits, and bearing areas. While TLS provides millimeter-level accuracy, UAV-based scanning enhances accessibility to hard-to-reach areas. However, occlusions and reflective steel surfaces can affect accuracy under certain conditions.
- *Corrosion and Section Loss Detection*: 3D scanning technologies successfully detected section loss and surface deterioration. However, it appears that their effectiveness depends on scanning resolution, surface conditions, and postprocessing methods. The study developed standardized workflows to improve consistency and reproducibility in condition assessments.
- *Data Processing and Structural Integration*: Large point cloud datasets require advanced filtering, segmentation, and modeling techniques for integration with finite element models (FEMs) and bridge management systems. The study provides guidelines to streamline data processing and analysis.
- *Field Application and Operational Limitations*: While 3D scanning reduces reliance on manual inspections, factors such as weather conditions, UAV flight restrictions, and equipment costs must be considered for practical field deployment.
- *Scanning Workflow Optimization*: The research produced guidelines for optimal scanning locations, data collection protocols, and quality control measures to improve efficiency and ensure reproducibility in bridge assessments.
- *Proposed Framework Validation*: A standardized framework was developed and validated for integrating 3D scanning data into bridge inspection workflows. This framework ensures consistent data collection, efficient processing, and seamless integration with structural evaluation models.

Implementation

To facilitate the integration of 3D scanning technologies into Indiana's bridge inspection program, the following recommendations are proposed:

- *Adoption of a Standardized Framework*: Implement the validated 3D scanning framework into routine inspections to ensure consistency, accuracy, and reliability in data collection and analysis.
- *Pilot Deployment on Targeted Bridges*: Conduct pilot studies on bridges with known structural deficiencies to refine scanning techniques, data processing workflows, and reporting procedures.
- *Training and Workforce Development*: Provide specialized training for bridge inspectors and asset managers on 3D scanning operations, data interpretation, and integration with structural analysis tools.
- *Integration with INDOT's Bridge Management System*: Ensure seamless incorporation of scanning outputs into existing bridge asset management platforms to support data-driven maintenance and rehabilitation planning.
- *Long-Term Scalability Assessment*: Conduct a cost-benefit analysis to determine the long-term feasibility of expanding 3D scanning across Indiana's bridge network and assess potential advancements in automated data processing and predictive maintenance capabilities.

By implementing these recommendations, Indiana's bridge inspection program can leverage 3D scanning technologies to improve accuracy, efficiency, and overall asset management decision-making. The findings of this study offer a structured approach to improving bridge inspection practices, reducing costs, and enhancing safety for Indiana's transportation infrastructure.

CONTENTS

LIST OF TABLES

LIST OF FIGURES

1. INTRODUCTION

1.1 Background

Bridge inspection and maintenance play a crucial role in ensuring the safety and longevity of transportation infrastructure. In the United States, bridges are required to undergo periodic inspections as mandated by the National Bridge Inspection Standards (NBIS; Indiana Department of Transportation [INDOT], 2022). Traditionally, bridge inspections have relied on manual visual assessments and conventional measurement tools, such as calipers, tape measures, and ultrasonic thickness gauges. While these methods have been widely used, they present significant limitations, including subjectivity, inconsistencies, and accessibility challenges, particularly for hard-to-reach structural components (Beainy et al., 2011; Horan et al., 2012; Wang et al., 2024). Additionally, manual inspections often require lane closures, increasing operational costs and posing safety risks to both inspectors and the traveling public (Khaloo et al., 2018; Tzortzinis et al., 2022).

Recent advancements in three-dimensional (3D) scanning technologies offer promising alternatives to traditional inspection methods by providing high-precision geometric data in a more efficient and automated manner. Technologies such as terrestrial laser scanning (TLS), close-range photogrammetry (CRP), and unmanned aerial vehicle (UAV)-based photogrammetry have demonstrated significant potential for structural assessment (Ameli et al., 2022; Miller et al., 2011; Pinto et al., 2020). These methods enable detailed data acquisition of bridge components, capturing corrosion-induced section loss, deformation, and cracks with minimal human intervention (Bolourian & Hammad, 2020; Yao & Song, 2023). The integration of these technologies into bridge inspections could improve accuracy, enhance efficiency, and reduce operational disruptions.

Despite the potential benefits, the application of 3D scanning in steel bridge inspections remains underdeveloped due to challenges in data processing, integration, and interpretation. There is a need for a systematic framework that enables the seamless transition from 3D scanning data to meaningful structural assessment outcomes. This research addresses this gap by developing a semiautomated framework that utilizes 3D scanning technologies for the inspection and residual strength estimation of steel girders. The framework aims to enhance the efficiency of bridge inspections while providing high-fidelity geometric models that can be integrated into finite element analysis (FEA) for structural evaluation.

1.2 Problem Statement and Objective

Bridges in Indiana and across the United States are subjected to periodic inspections to ensure their structural integrity and safety (INDOT, 2022). Traditional bridge inspection methods rely heavily on visual assessments and manual measurements, which are often labor intensive, time consuming, and highly dependent on the experience of the inspector (Beainy et al., 2011; Horan et al., 2012). These methods introduce subjectivity and potential inconsistencies in the assessment process leading to variations in reported conditions (Khaloo et al., 2018; Tzortzinis et al., 2022). Additionally, accessing critical structural components, such as girders located beneath the deck or within confined spaces, poses significant challenges and safety risks to inspectors (Mohammadi et al., 2021; Wang et al., 2024). The increasing demand for efficient, accurate, and automated inspection techniques highlights the limitations of current practices and underscores the need for advanced technological solutions (Jin et al., 2021).

The adoption of 3D scanning technologies presents a promising approach to overcoming these challenges. Techniques such as TLS, CRP, and drone-based scanning have demonstrated the capability to capture high-precision geometric data of bridge components (Gyetvai et al., 2018; Pinto et al., 2020; Yao & Song, 2023). However, despite the availability of these technologies, several key challenges hinder their widespread implementation for bridge inspections. These challenges include data processing complexities, accuracy limitations in field conditions, difficulties in integrating point cloud data (PCD) with structural analysis models, and the lack of standardized guidelines for practical use in steel bridge inspections (Khaloo et al., 2018; Omar & Nehdi, 2017). Without a systematic approach, these technologies remain underutilized, preventing their full potential from being realized in routine bridge management (INDOT, 2022; Metni & Hamel, 2007; Miller et al., 2011).

The objective of this project is to develop a generalized framework for utilizing 3D scanning technologies in bridge inspections, specifically focusing on the assessment of steel girders and residual strength estimation. This framework aims to:

- Evaluate the accuracy and feasibility of different 3D scanning technologies for bridge inspections;
- Develop optimal scanning strategies tailored to different bridge types and conditions in Indiana;
- Establish a workflow for integrating 3D PCD into finite element models (FEMs) for strength assessment; and
- Develop a set of guidelines for INDOT to facilitate the adoption of 3D scanning in routine bridge inspections.

By addressing these objectives, this project will provide a structured and reproducible methodology for incorporating 3D scanning into bridge inspections, improving data reliability, reducing manual effort, and enhancing the overall decision-making process for infrastructure management.

1.3 Research Approach

To develop a generalized framework for 3D scanning in bridge inspections, this project uses a multiphase approach. It integrates literature review, experimental investigations, numerical modeling, and field validation.

The first phase involves a literature review to evaluate 3D scanning technologies for bridge inspections. It compares techniques like terrestrial laser scanning (TLS), close-range photogrammetry (CRP), and UAV-based photogrammetry in terms of accuracy, efficiency, cost, and practical implementation challenges. Commercial scanning devices are also reviewed for optimal hardware configurations.

The second phase focuses on experimental investigations to assess scanning accuracy and applicability. Controlled laboratory experiments are conducted using corroded steel girders at Bowen Laboratory to evaluate different scanning methods under varying conditions. The results are validated against conventional measurement techniques to establish benchmarks.

The third phase involves developing a data processing pipeline for integrating PCD into structural analysis models. This includes automated segmentation, 3D model conversion, and residual strength estimation using FEM. Python scripts extract section loss measurements, which are applied to develop FEMs predicting corroded girders' remaining load-bearing capacity. Numerical results are validated against experimental data.

The fourth phase extends research to field implementation, scanning bridge structures in Indiana with optimized 3D scanning strategies. Real-world bridge inspections test integrating 3D scanning into routine workflows. Key operational parameters, such as UAV flight path optimization and environmental considerations, are documented.

Finally, practical guidelines and recommendations for 3D scanning in bridge inspections are developed. These cover technology selection, field procedures, data processing, and integration with INDOT bridge management systems. The final report provides a structured approach for adopting 3D scanning technologies for enhanced structural assessments.

1.4 Research Scope

This project aims to develop a systematic framework for integrating 3D scanning technologies into bridge inspections, specifically targeting steel girders and residual strength estimation. The research will evaluate, implement, and validate 3D scanning techniques in controlled laboratory settings and real-world bridge environments in Indiana.

The project investigates multiple 3D scanning techniques, including terrestrial laser scanning, close-range photogrammetry, and drone-based photogrammetry, to assess their feasibility for geometric data collection, defect identification, and structural assessment. It addresses corrosion-induced section loss, deformation, and material degradation in steel girders, which are critical factors in evaluating bridge structural integrity. The study also explores multitemporal data integration to enhance long-term monitoring of structural deterioration.

Beyond data collection, the project involves data processing and structural analysis, including automated point cloud segmentation, conversion into 3D solid models, and finite element modeling for residual strength estimation. It also optimizes scanning parameters to improve accuracy and efficiency.

The study includes field validation through full-scale bridge inspections, incorporating lessons from controlled laboratory experiments. Bridges in Indiana will be scanned using the optimized framework to assess its real-world applicability. This ensures the framework's practicality, scalability, and adaptability to diverse bridge types and conditions.

Finally, the study develops guidelines and recommendations for implementing 3D scanning in routine bridge inspections. These guidelines address technology selection, scanning procedures, data processing workflows, and integration strategies for INDOT bridge management systems. By establishing a structured methodology, the research aims to facilitate the adoption of 3D scanning technologies, enhancing bridge condition assessments' accuracy, efficiency, and reliability.

1.5 Structure of the Report

This report provides a comprehensive overview of research on 3D scanning technologies for bridge inspection and their implementation. It explores existing technologies, their applications, and challenges for steel girder assessments. The research team developed a systematic framework through field scanning activities, testing equipment, evaluating conditions, optimizing path planning, and performing feasibility checks. The framework includes technology selection, field preparation, postprocessing, and data management for repeatability and reliability. The methodology details 3D solid model conversion, residual strength estimation, and field implementation strategies. The report concludes with practical implementation of the framework and guidelines, and broader implications for bridge inspection and management.

2. LITERATURE REVIEW

2.1 Background of 3D Scanning Technologies

3D scanning technologies have emerged as powerful tools for capturing high-resolution geometric data of infrastructure elements, including bridges (Bolourian & Hammad, 2020; Chen et al., 2019). These technologies utilize laser scanning, photogrammetry, or a combination of both to create precise digital models of structural components, facilitating automated defect detection, damage assessment, and structural analysis (Ameli et al., 2022; Lu & Brilakis, 2017). In the context of bridge inspection, 3D scanning technologies offer significant advantages over traditional manual inspection methods by providing rapid, non-contact, and high-precision data acquisition while reducing human subjectivity and safety risks (Khaloo et al., 2018). This section provides background of 3D scanning technologies being used in the industry.

2.1.1 Terrestrial Laser Scanning (TLS)

TLS, also known as ground-based light detection and ranging (LiDAR), employs LiDAR sensors to capture millions of points in a three-dimensional space. TLS devices, such as Faro Focus and Trimble TX series, generate high-density point clouds that accurately represent structural geometries. These scanners are often mounted on tripods and positioned at multiple locations around a bridge to obtain comprehensive coverage. TLS is particularly effective for large-scale data collection, detecting surface deformations, and measuring corrosion-induced section loss in steel girders (Wang et al., 2024). However, its primary limitations include high equipment costs, sensitivity to ambient lighting conditions, and line-of-sight constraints that may require multiple scan positions (Elkawas et al., 2017).

2.1.2 Close-Range Photogrammetry (CRP)

CRP is a camera-based scanning technique that reconstructs 3D models by processing multiple overlapping images of an object. Unlike LiDAR, which relies on laser pulses, CRP uses computer vision algorithms to extract spatial information from photographs. The technique is widely adopted due to its affordability, portability, and ease of use (Pinto et al., 2020). CRP has been successfully implemented for bridge inspections, crack detection, and section loss measurements, demonstrating comparable accuracy to LiDAR when high-quality images are captured under controlled conditions (Jin et al., 2021; Popescu et al., 2019). However, challenges such as camera calibration, lighting inconsistencies, and the need for stable image alignment can affect data quality and accuracy (Yiqiu et al., 2014).

2.1.3 Drone-Based Photogrammetry and LiDAR

UAVs, or drones, equipped with photogrammetry cameras or LiDAR sensors, provide a highly flexible and efficient solution for bridge inspections, particularly for hard-to-reach areas such as the underside of bridge decks, high steel girders, and confined spaces. Advanced drones, such as DJI Matrice 300 RTK and DJI Avatar2, offer real-time kinematic (RTK) positioning, enabling precise georeferencing of collected data. Drone-mounted LiDAR scanners can capture detailed structural features with centimeter-level accuracy, while high-resolution cameras support automated defect recognition and 3D reconstruction (Khaloo et al., 2018; Wang et al., 2024). The main advantages of UAV-based scanning include rapid deployment, minimal disruption to traffic, and enhanced coverage of complex bridge geometries (Lu & Brilakis, 2017). However, limitations such as weather dependency, flight time restrictions, and regulatory compliance (e.g., Federal Aviation Administration (FAA) Part 107 certification) must be carefully considered when deploying drones for bridge inspections.

2.2 Comparison of 3D Scanning Technologies

Each 3D scanning technology offers distinct advantages and limitations based on inspection objectives, environmental conditions, and required accuracy levels (Beainy et al., 2011). While TLS provides the highest accuracy for localized measurements (Gyetvai et al., 2018; Tzortzinis et al., 2022), CRP offers a cost-effective alternative with reasonable accuracy under controlled conditions (Pinto et al., 2020; Popescu et al., 2019), and drone-based photogrammetry/LiDAR enhances accessibility and efficiency for large-scale inspections, particularly in hard-to-reach areas (Ameli et al., 2022; Wang et al., 2024). The selection of the most suitable 3D scanning technology depends on multiple factors, including bridge type, environmental conditions, accuracy requirements, and budget constraints (INDOT, 2022; Khaloo et al., 2018). The selection of an appropriate 3D scanning technology depends on factors such as bridge type, structural complexity, budget constraints, and data processing requirements (INDOT, 2022).

This project evaluates these technologies through controlled laboratory experiments and field implementations to determine their feasibility and effectiveness in steel girder inspections and residual strength estimation (Pinto et al., 2020; Wang et al., 2024). The insights gained from these evaluations will guide the development of a standardized framework and guidelines for integrating 3D scanning into routine bridge inspections, ensuring accuracy, efficiency, and reproducibility in bridge condition assessments (Yao & Song, 2023).

2.3 Applications of 3D Scanning in Bridge Inspection

3D scanning technologies, such as TLS, CRP, and UAV-based LiDAR scanning, provide high-resolution geometric data of bridge components, enabling detailed assessments of section loss, deformation, corrosion, and other structural deterioration (Chen et al., 2019; Lu & Brilakis, 2017). Unlike manual inspections, which depend on the experience and judgment of inspectors, 3D scanning technologies generate objective and repeatable digital records of bridge conditions, reducing inconsistencies and improving decision making in maintenance and rehabilitation planning (Jáuregui et al., 2006; Mohammadi et al., 2021; Pinto et al., 2020).

Several studies have demonstrated the effectiveness of 3D scanning technologies in automating bridge inspections and improving assessment accuracy (Popescu et al., 2019; Wang et al., 2024). TLS has been successfully used to capture precise geometric details of bridge elements, including girder deformations, crack propagation, and misalignments (Gyetvai et al., 2018; Tzortzinis et al., 2022). Research has shown that TLS can achieve millimeter-level accuracy, making it suitable for detailed bridge condition monitoring over time. However, TLS requires multiple scanning positions and manual post-processing to align point clouds, which can be labor-intensive (Elkawas et al., 2017).

CRP has gained popularity as a cost-effective alternative to TLS, allowing inspectors to create accurate 3D models from a series of overlapping images (Jiang & Jáuregui, 2010; Khaloo et al., 2018). Studies have demonstrated that CRP can be used to detect section loss in steel girders, estimate corrosion depth, and assess overall bridge geometry (Pinto et al., 2020). The main advantages of CRP include affordability, portability, and the ability to capture high-resolution data with consumer-grade cameras (Jin et al., 2021). However, challenges related to image alignment, lighting conditions, and the need for stable reference points must be addressed to ensure reliable results (Yiqiu et al., 2014).

Drone-based photogrammetry and LiDAR scanning have emerged as powerful tools for inspecting hard-to-reach areas of bridges, such as underside girder sections, deck soffits, and confined spaces (Ameli et al., 2022; Wang et al., 2024). UAV-mounted LiDAR can rapidly scan large bridge structures and generate high-fidelity 3D models, significantly reducing inspection time while improving data completeness. Recent studies have highlighted the ability of drones to perform bridge assessments without requiring lane closures or scaffolding, improving both safety and efficiency (Lu & Brilakis, 2017; Pinto et al.,

2020). However, flight restrictions, environmental factors, and regulatory compliance pose challenges for widespread adoption (Omar & Nehdi, 2017).

2.4 Challenges and Gaps in Adopting These Technologies for Steel Girders

Although 3D scanning technologies provide numerous advantages, their implementation in steel bridges presents unique challenges that differ from other bridge types (Barth & Wu, 2006; Mohammadi et al., 2021). Steel bridges experience corrosion, section loss, and fatigue cracking, making high-resolution scanning and precise defect detection crucial for structural assessment (Jiang & Jáuregui, 2010; Tzortzinis et al., 2022).

2.4.1 Corrosion and Section Loss Detection

Steel girders are susceptible to corrosion, leading to section loss that affects load-carrying capacity. While TLS and UAV-based LiDAR can detect large-scale section loss, capturing small pitting corrosion and early-stage deterioration remains challenging (Elkawas et al., 2017). Integrating advanced processing techniques such as AI-based corrosion detection and multispectral imaging could enhance accuracy (Lu & Brilakis, 2017; Wang et al., 2024).

2.4.2 Challenges in Capturing Thin Structural Components

Steel bridges have thin plate elements, stiffeners, and intricate connections, making accurate point cloud generation difficult. TLS and CRP face occlusion issues, leading to missing data points in shadowed or confined spaces (Popescu et al., 2019). UAVs with oblique-angle scanning and multiview photogrammetry have shown promise in addressing these gaps (Pinto et al., 2020).

2.4.3 High Reflectivity of Steel Surfaces

Unlike concrete, steel surfaces are highly reflective, which can cause errors in LiDAR-based scanning. Laser beam reflections may lead to incorrect distance measurements, requiring postprocessing adjustments (Ameli et al., 2022). Researchers have explored polarized LiDAR scanning and optimized sensor configurations to minimize reflectivity-induced errors.

2.4.4 Finite Element Model (FEM) Integration Challenges

For structural analysis, 3D scanning data must be seamlessly integrated into FEMs for accurate residual strength evaluation. However, PCD often require manual mesh refinement to create FEM-compatible models (Jiang & Jauregui, 2010). Automated meshing techniques and AI-driven FEM generation could enhance efficiency and accuracy (Wang et al., 2024).

This project tackles these challenges by evaluating different 3D scanning technologies, developing a systematic framework for bridge inspection, and proposing guidelines for implementation. By bridging the gap between technology development and field applications, this research aims to support transportation agencies, such as INDOT, in adopting 3D scanning for more reliable and data-driven bridge management practices.

3. RESEARCH APPROACH: DEVELOPMENT OF 3D SCANNING GUIDELINE

Developing standardized scanning guidelines ensures consistent data quality, operational efficiency, and reliable structural assessments across diverse bridge types. These guidelines provide structured protocols for field data collection, improving bridge inspection accuracy, efficiency, and repeatability.

This chapter describes the systematic approach taken to develop the scanning guidelines, including laboratory testing, field validation, and data processing evaluations. The research team conducted controlled experiments at Bowen Laboratory and field scanning activities across multiple bridge sites in Indiana to assess different scanning technologies, environmental influences, and operational challenges. Through these evaluations, the team refined:

- Testing multiple 3D scanning technologies, including terrestrial laser scanning (TLS), close-range photogrammetry (CRP), and UAV photogrammetry, to determine optimal configurations for different bridge conditions;
- Assessing the impact of environmental factors, such as lighting conditions, surface reflectivity, and atmospheric variations, on data quality;
- Optimizing data acquisition strategies by refining scan locations, overlap rates, and scanning angles to minimize occlusions and enhance measurement accuracy; and
- Validating measurement accuracy under various field conditions by comparing 3D scanning results to ground-truth reference measurements.

Based on the findings from these evaluations, the research team developed scanning guidelines focused on four key components:

1. *Equipment Selection*: Systematic evaluation of scanning technologies (TLS, CRP, and UAV-based systems) for different bridge types and inspection needs.
2. *Path Planning and Optimization*: Development of scanning protocols through laboratory testing and field validation to optimize scanning efficiency and data quality.
3. *Field Implementation*: Deployment of scanning methods in real bridge environments, accounting for logistical and operational factors that impact data collection.
4. *Quality Control*: Establishment of prescanning assessment procedures, verification methods, and postprocessing validation techniques to ensure consistent and accurate results.

The following sections detail each of these critical elements, providing specific recommendations and best practices. The finalized guidelines are provided in Chapter 4.

3.1 Equipment Selection

The selection of an appropriate 3D scanning technology is vital for accurately detecting section loss in steel girders. Following an extensive literature review, the research team

evaluated TLS and CRP based on measurement accuracy, feasibility, and data processing requirements. The evaluation approach consisted of three phases:

- First, conducting controlled laboratory tests using an 18-ft W-section specimen at Bowen Laboratory to assess resolution, scanning configurations, and reliability;
- Second, analyzing the comparative results to identify the most suitable technology; and
- Third, performing multiple outdoor field tests to refine scanning protocols for real-world conditions.

This systematic approach led to the adoption of drone-based photogrammetry as the preferred method, offering an optimal balance of accuracy, efficiency, and practicality for field operations.

3.1.1 Comparison of TLS and CRP

After literature review, the research team identified TLS and CRP as the most suitable technologies for inspecting steel bridge girder members. The initial testing phase focused on determining each technology's precision for section loss detection (1–2 mm). To compare under optimal conditions, an 18-ft W-section specimen was set up at Bowen Laboratory. To provide a brief overview of each method's core attributes, Table 3.1 compares TLS and CRP in terms of resolution, operating range, capture configurations, and processing requirements.

A comprehensive testing protocol was developed to evaluate each technology's performance under controlled scanning conditions, including consistent lighting. For the TLS assessment, a FARO Focus 3D Scanner was deployed at three scanning locations per side and two different elevations, ensuring complete coverage of the W-section, minimizing shadowing, and maintaining uniform point density. Figure 3.1 illustrates the TLS setup, and Figure 3.2 shows the resulting point cloud.

By contrast, CRP required a more complex data acquisition strategy using a Sony α7M4 full-frame mirrorless camera. The image capture protocol spanned four distinct elevation layers—positioned above the girder, at mid-upper height, at mid-lower height, and below the girder—with both surrounding and oblique views of the W-section, thus covering critical areas such as web-flange intersections and potential section loss regions. This systematic multilevel approach ensured comprehensive documentation of the entire structural element while minimizing shadowed or occluded areas in the final reconstruction.

TABLE 3.1
Comparison of TLS and CRP Technologies.

Feature	Terrestrial Laser Scanner (FARO Focus 3D)	Close-Range Photogrammetry (Sony α7M4)
Resolution	44 MPts/Scan	33MP sensor resolution
Operating Range	65 ft optimal	3´–7´ testing range
Capture Configuration	6 scan positions (3 per side × 2 elevations)	4 elevation layers with surrounding and oblique views
Processing Requirements	Direct point cloud generation	Photogrammetric reconstruction required

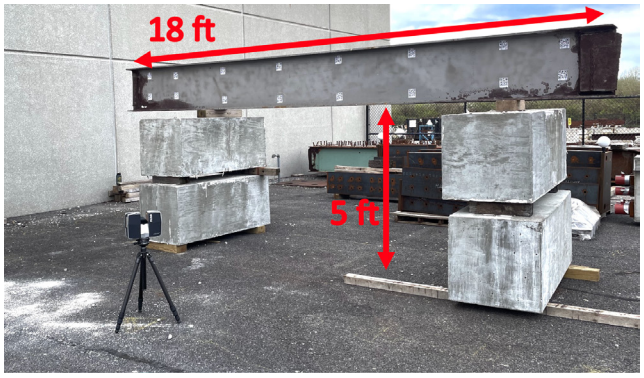

Figure 3.1 TLS Scanning Setup.

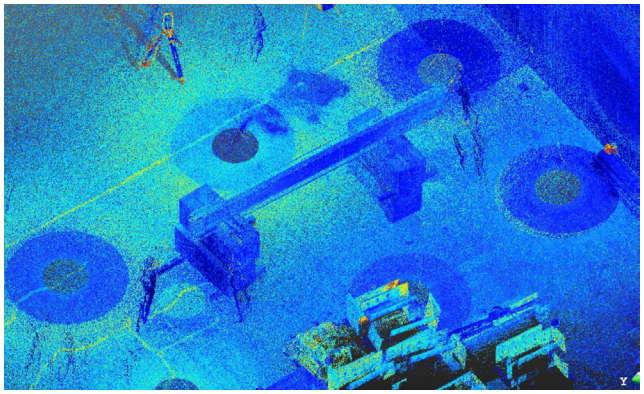

Figure 3.2 TLS Scanning Result.

Figure 3.3 shows the CRP scanning experiment in progress, and Figure 3.4 shows its corresponding photogrammetric reconstruction.

To investigate how image density influences model accuracy, the research team conducted three imaging scenarios for CRP:

1. A high-density capture of 1,000 images at a 3–7 ft range
2. A medium-density capture of 350 images at a 5–7 ft range
3. A minimal capture of 100 images at a 7 ft range

Figure 3.3 CRP Scanning Experiments.

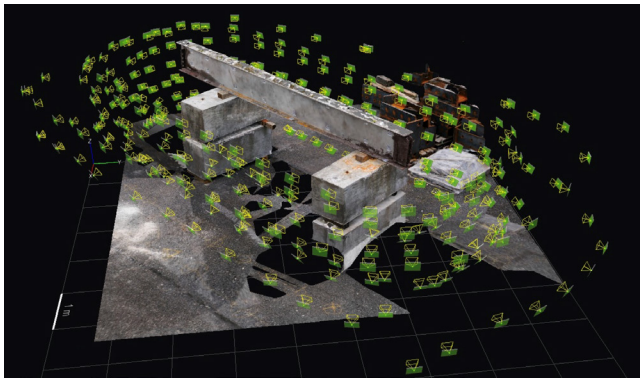

Figure 3.4 CRP Scanning Result.

Figure 3.5 Measurement Locations and QR Code Targets on the Steel Girder.

To establish ground truth for validation, the team used caliper readings, ultrasonic thickness measurements, and total station surveys. These references provided a robust baseline for comparing the accuracy and reliability of each technology. Figure 3.5 illustrates the labeling of sample measurement locations (A1, A2, etc.) and the placement of QR code targets on the W-section, facilitating accurate point cloud registration and consistent measurement across different methods. These QR codes served dual purposes: they provided scaling constraints for the photogrammetric reconstruction process, ensuring dimensional accuracy of the resulting model, and their centers were used as precise reference points for thickness validation, allowing direct comparison between ultrasonic sensor measurements and thickness values derived from the photogrammetric model.

Table 3.2 presents local thickness measurements (for both flange and web locations), showing how TLS and CRP values

TABLE 3.2
Comparison of All Measurement Methods and Results for W-Section Scanning.

Measurement Point (Location)	Ground Truth (in.)	Method	TLS Results Value (in.) [Diff %]	CRP Results 3ft (in.) [Diff %]
A1	0.59	Caliper	0.57 [2.58%]	0.62 [5.0%]
A2	0.59	Caliper	0.58 [1.64%]	0.63 [6.0%]
A3	0.52	Caliper	0.55 [-6.37%]	0.32 [-38.0%]
A4	0.526	Caliper	0.58 [-10.33%]	0.49 [-7.0%]
A5	0.21	Caliper	0.23 [-9.67%]	0.20 [-5.0%]
A6	0.303	Caliper	0.29 [4.50%]	0.31 [3.0%]
A7	0.22	Caliper	0.26 [-16.50%]	0.10 [-52.0%]
A8	0.251	Caliper	0.26 [-3.99%]	0.22 [-11.0%]
A9	0.606	Caliper	0.59 [2.29%]	0.58 [-4.0%]
t30	0.61	Ultrasonic	N/A	0.60 [-1.0%]
t11	0.43	Ultrasonic	0.55 [-28.91%]	0.44 [2.0%]
c9	0.424	Ultrasonic	0.54 [-26.93%]	0.44 [3.0%]
c5	0.433	Ultrasonic	0.57 [-31.57%]	0.44 [1.0%]
c11	0.426	Ultrasonic	0.54 [-27.91%]	0.44 [4.0%]
c1	0.428	Ultrasonic	0.56 [-31.45%]	0.47 [9.0%]
c7	0.432	Ultrasonic	0.56 [-28.96%]	0.47 [8.0%]
c3	0.425	Ultrasonic	0.54 [-27.47%]	0.43 [1.0%]

TABLE 3.3
Comparison of Global Dimensional Measurements.

Distance b/w Ref. Points	Total Station (in.)	TLS (in.) [Diff %]	CRP (all distances) [Diff %]
C3–C7	89.25	89.32 [0.07%]	89.21 [0.00%]
C7–C1	62.50	62.57 [0.11%]	62.60 [0.00%]
C3–C1	149.25	149.24 [0.01%]	149.17 [0.00%]

compare to their respective ground truth measurements. The data reveal that TLS measurements deviated between 1.64% and 16.50% for flange locations (points A1, A2, A4, A6, A8, A9), while showing larger discrepancies of 26.93% to 31.57% for web thickness measurements (points t11, c1-c11). In contrast, CRP demonstrated better performance for web thickness measurements with deviations typically ranging from 1% to 9%, though it showed more variability in flange measurements, particularly at points A3 and A7 with -38.0% and -52.0% deviations, respectively. Overall, these results indicate that while TLS provides more consistent flange measurements, CRP tends to achieve higher accuracy in capturing web thickness values, which are critical for section loss assessment in bridge inspections.

TLS excelled in global dimensional measurements, with deviations below 0.4% relative to total station data, as shown in Table 3.3. In contrast, CRP showed variability at specific flange points but achieved higher accuracy in web thickness assessments (e.g., A3 and A7) with deviations typically ranging from 1% to 9%, while maintaining comparable accuracy in global dimensions (Table 3.2).

These findings highlight the strengths of TLS and CRP. TLS provides robust global dimensional accuracy and consistent flange measurements, while CRP accurately captures web thickness at closer ranges. A hybrid approach using both may

yield the most comprehensive measurement of steel girder geometry for bridge inspections.

3.1.2 Implementation of Drone-Based Photogrammetry

The research team's decision to prioritize drone-based photogrammetry for bridge inspections was solidified by initial technology evaluation findings. Drone-based photogrammetry offers practical advantages over TLS. TLS requires multiple ground setups and direct access to bridge elements, making it time consuming and potentially disruptive. Drones can access hard-to-reach areas easily, reducing setup time and minimizing traffic disruptions. Additionally, CRP's successful validation at a 3 ft capture distance aligns with drone operation parameters, suggesting field replicability of measurement quality.

To address these requirements, the research team selected the DJI Matrice 300 RTK platform paired with the Zenmuse P1 camera system. The research team selected the DJI Matrice 300 RTK platform with the Zenmuse P1 camera system to address these requirements. The Zenmuse P1's 45 MP full-frame sensor with a fixed-focus 35 mm lens provides enhanced low-light performance and a wider dynamic range than smaller sensors, making it ideal for inspecting under-bridge areas with suboptimal lighting.

As illustrated in Figure 3.6 and Figure 3.7, the DJI Matrice 300 RTK includes the following features that are essential for bridge inspection activities:

- RTK Positioning System offers half-inch-level accuracy for georeferenced data collection.
- Upward Gimbal Mounting Capability enables inspection of under-bridge areas by allowing the camera to face upward
- Advanced Obstacle Avoidance Systems enhances operational safety when maneuvering near structural components
- Extended Flight Time (up to 55 minutes) allows for comprehensive data collection without frequent battery swaps
- IP45 Weather Resistance Rating facilitates safe operation in adverse weather conditions
- Hot-Swappable Battery System minimizes downtime and supports uninterrupted inspection workflows

These combined capabilities address key bridge inspection challenges, especially limited accessibility and the need for accurate data. Drone-based photogrammetry with a robust RTK-enabled platform efficiently gathers critical structural information, minimizing traffic impact.

Photogrammetry for Bridges' Complex Structures are unique challenges compared to traditional photogrammetry applications. While typical photogrammetry deals with exterior surfaces in controlled environmental conditions, bridge inspection captures complex, interconnected surfaces in confined areas like webs, flanges, bracings, and other connections. This structural complexity requires collecting both global geometric data and detailed information in critical regions like web-flange intersections to minimize section loss.

Environmental factors complicate photogrammetry in bridge settings, affecting data quality and efficiency. Unlike architectural photography, bridge inspections often have inconsistent

Figure 3.6 DJI Matrice 300 RTK.

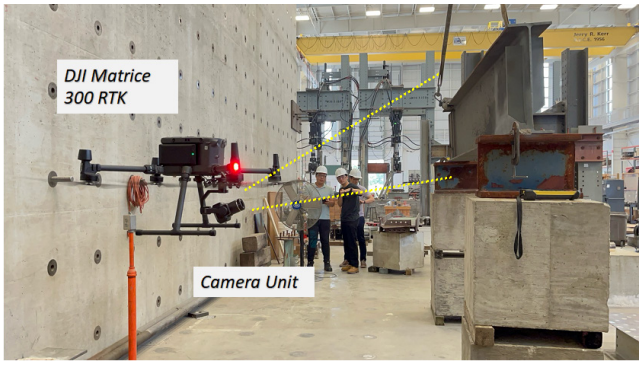

Figure 3.7 Drone Attitude During Flight.

or low-light environments beneath deck structures. These varying lighting conditions can cause brightness differences along the same girder, as shown in Figure 3.8. Smooth, painted steel surfaces provide few distinct features for reconstruction, increasing alignment errors. Wind-induced motion, especially in confined spaces, can compromise image quality by causing camera shake or misalignment.

The precision requirements for bridge inspection exceed those of most typical photogrammetric applications. Detecting millimeter-scale section loss and accurately measuring remaining material thickness are critical for structural assessments,

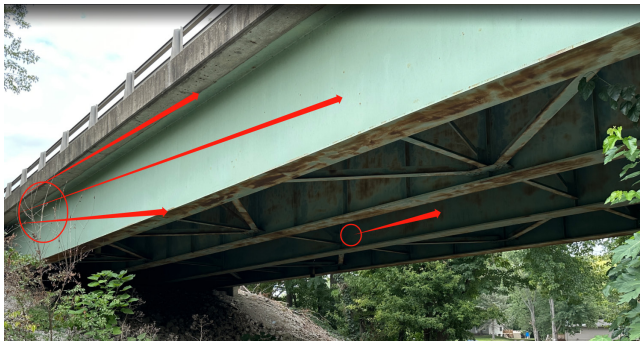

Figure 3.8 Outside W-section is Brighter Than Inside W-Section Due to Different Light Conditions.

TABLE 3.4
Overview of Key Parameters and Validation Metrics for Bridge Photogrammetry for Laboratory Testing Phase.

Category	Parameters to Optimize	Validation Metrics
Coverage Pattern	Image overlap ratios (front/side)	• Point cloud density
	Multielevation layer spacing	• Surface coverage completeness
	Oblique angle effectiveness	• Feature reconstruction quality
Distance & Resolution	Working distance ranges	• Section loss detection accuracy
	Camera resolution settings	• Thickness measurement precision
	Surface reflection handling	• Point cloud noise levels

including load rating adjustments and long-term deterioration monitoring. These demands imply that every aspect of the scanning process—from hardware selection to field execution—must meet stringent accuracy typical to produce reliable results.

Addressing these challenges requires careful consideration of key parameters for successful scanning protocols. Image capture strategies may need higher overlap ratios than typical photogrammetry for robust feature matching, especially in areas with limited texture. Multiple viewpoints help capture surface details in potential corrosion regions. Working distances must be optimized for sufficient image resolution without contact or collisions, especially beneath deck structures with restricted clearances. Resolution settings should balance detail and data volume for efficient processing and analysis.

To guide this process, the research team developed a comprehensive guideline with four primary phases: Laboratory Testing (Table 3.4), Field Implementation (Table 3.5), Environmental (Table 3.6), and Site-Specific (Table 3.7). Each phase addresses specific challenges, drawing from preliminary research and bridge engineering standards.

Several parameters stand out as influential in bridge inspection guidelines. Laboratory-based coverage patterns and working distance experiments establish accuracy for section loss detection. Field implementation protocols ensure under-deck scanning and girder complexity are addressed. Environmental factors like lighting and wind affect data integrity and safety.

TABLE 3.5
Overview of Key Parameters and Validation Metrics for Bridge Photogrammetry for Field Implementation Testing Phase.

Category	Parameters to Optimize	Validation Metrics
Scanning Strategy	Component-specific patterns	• Coverage efficiency
	Vertical surface methods	• Data completeness
	Under-deck approaches	• Time efficiency
	Complex geometry protocols	• Safety compliance
Operational Protocol	Flight zone requirements	• Setup time
	Battery management	• Mission success rate
	Mission segmentation	• Data quality consistency
	Safety buffers	• Risk mitigation effectiveness

TABLE 3.6
Overview of Key Parameters and Validation Metrics for Bridge Photogrammetry for Environmental Testing Phase.

Category	Parameters to Optimize	Validation Metrics
Lighting Management	Shadow compensation	Image quality metrics
	Time-of-day planning	Exposure consistency
	Exposure settings	Feature detectability
Weather Limits	Wind thresholds	Position stability

TABLE 3.7
Overview of Key Parameters and Validation Metrics for Bridge Photogrammetry for Site-Specific Testing Phase.

Category	Parameters to Optimize	Validation Metrics
Physical Constraints	Clearance requirements	Access feasibility
	Obstacle avoidance	Coverage completeness
Operational Factors	Traffic coordination	Disruption minimization
	Time windows	Schedule efficiency

Site-specific considerations like traffic management and clearance restrictions impact data collection feasibility. These critical elements are a focused in the resulting recommendations for routine bridge inspections.

3.2 Path Planning and Optimization

Optimizing drone-based bridge inspections requires a systematic approach ensuring complete coverage without compromising data quality. This section details iterative scanning protocol development through laboratory and field testing. At Bowen Laboratory, baseline flight parameters were established under controlled conditions, then refined in real bridge environments. By iterating between controlled experiments and field validations, comprehensive flight planning strategies were formulated balancing coverage completeness, data accuracy, and operational efficiency.

3.2.1 Laboratory Testing Phase

Developing optimal path planning strategies for drone-based bridge inspection requires systematic evaluation in controlled conditions before field implementation. Extensive laboratory testing at Bowen Laboratory established baseline parameters

TABLE 3.8
Overview of Scanning Iterations Conducted at Bowen Laboratory.

Scanning Date	Total Photos	Key Parameters	Primary Objectives	Key Findings & Issues
07-17-2023 (1st)	569	• ISO: 1600 • Shutter: 1/250 • Aperture: 5.6 • Exposure: 0 • No supplementary lighting	• Initial drone-based scanning test • Evaluate basic circular flight path	• 54% lost/disconnected images • Poor edge connectivity • Insufficient coverage at transitions
07-24-2023 (2nd)	850	• ISO: 1600 • Shutter: 1/250 • Aperture: 5.6 • Exposure: 0 • No supplementary lighting	• Improve edge coverage • Enhance model quality • Test multilevel scanning	• Reduced lost images to 2% • Better edge coverage • Excessive redundant data • Middle section focus issues
08-10-2023 (3rd)	294	• ISO: 100 • Shutter: 1/80 • Aperture: 2.8 • Under exposure: -2.8 • Back and edge lighting added	• Optimize camera parameters • Implement sparse capture strategy • Validate lighting setup	• 0% lost images • Efficient data collection • Complete coverage achieved

and validated scanning protocols. The testing focused on controlled environment experiments, coverage optimization studies, and validating parameters in a controlled setting.

The controlled environment experiments used an 18 ft W-section specimen under standardized conditions. Drone-based systems struggled to achieve consistent coverage, especially in confined areas. Unlike handheld CRP, drone operations require careful flight path stability, obstacle avoidance, and maintaining a consistent distance to the structure. To address these complexities, the research team iteratively tested and refined scanning protocols.

Between July and August 2023, three iterations refined the path planning strategy. Lab testing details are below. Table 3.8 summarizes each iteration's flight path approach, captured images, and key findings.

3.2.2 Iteration 1 (July 17, 2023)

This initial iteration employed a circular flight path approach similar to conventional photogrammetry, capturing 569 images. However, 54% of these images failed to integrate into the final model due to inadequate overlap and insufficient edge coverage. Figure 3.9, Figure 3.10, and Figure 3.11 illustrate the flight path (indicated by green camera positions) and the resulting 3D model, highlighting sparse and uneven point cloud distribution, especially along the edges of the W-section.

3.2.3 Iteration 2 (July 24, 2023)

In response to the connectivity problems encountered in Iteration 1, the second iteration applied a multilevel scanning strategy and expanded the total image count to 850, reducing disconnected images to 2%. While this approach significantly enhanced coverage, it also introduced data redundancy and proved less efficient in terms of processing time. Figure 3.12, Figure 3.13, and Figure 3.14 show the flight path layout, indicating a more structured distribution of camera positions, along with corresponding model views that reveal a denser, more complete point cloud.

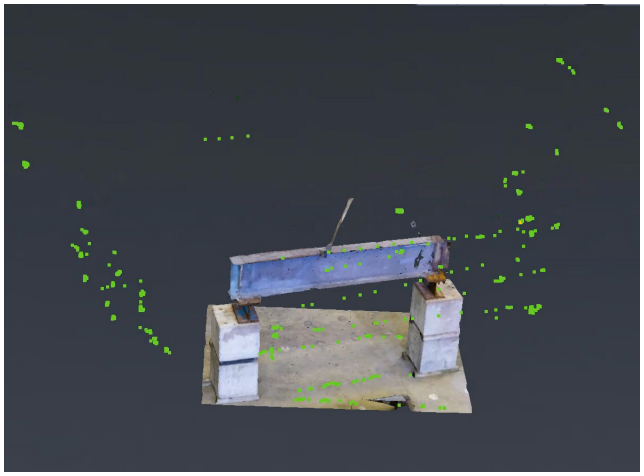

Figure 3.9 Flight Path Visualizations (Green Camera Positions). Scanning Date: July 17, 2023, Circular Flight Path.

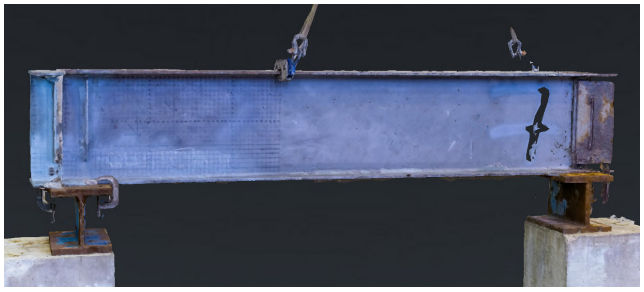

Figure 3.10 Horizontal Views of the Resulting 3D Models. Scanning Date: July 17, 2023, Circular Flight Path.

3.2.4 Iteration 3: (August 10, 2023)

The final iteration achieved optimal results by refining the capture strategy and reducing the total images to 294 while still maintaining complete model coverage. This was accomplished through careful optimization of flight parameters,

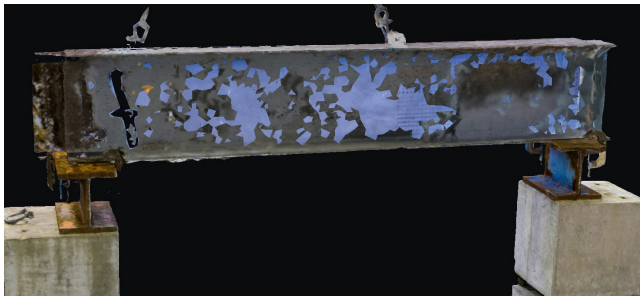

Figure 3.11 Vertical Views of the Resulting 3D Models. Scanning Date: July 17, 2023, Circular Flight Path.

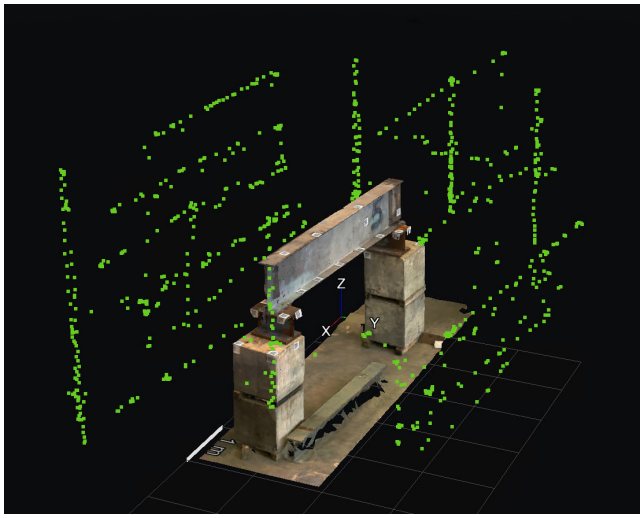

Figure 3.12 Flight Path Visualizations (Green Camera Positions). Scanning Date: July 24, 2023, Multilevel Scanning Approach.

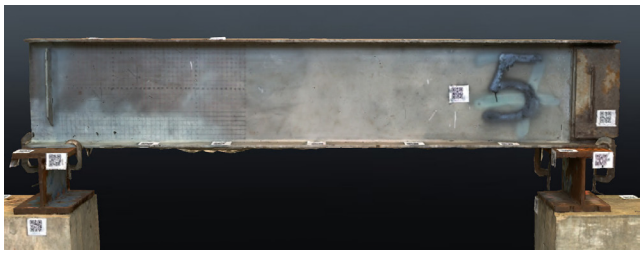

Figure 3.13 Horizontal Views of the Resulting 3D Models. Scanning Date: July 24, 2023, Multilevel Scanning Approach.

camera settings, and lighting conditions. The camera parameters were adjusted from their initial values (ISO 1600, shutter speed 1/250, aperture f/5.6) to more effective settings (ISO 100, shutter speed 1/80, aperture f/2.8, exposure compensation –2.8). Additionally, strategic lighting placed at the rear and edges of the specimen enhanced image clarity and improved reconstruction accuracy. Figure 3.15, Figure 3.16, and Figure 3.17 display the final flight path arrangement and corresponding 3D model views, emphasizing a uniform, consistent point cloud without excessive redundancy.

Figure 3.14 Vertical Views of the Resulting 3D Models. Scanning Date: July 24, 2023, Multilevel Scanning Approach.

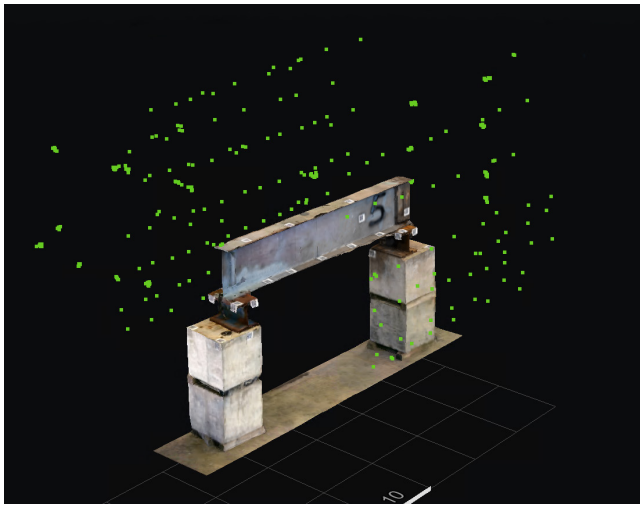

Figure 3.15 Flight Path Visualizations (Green Camera Positions). Scanning Date: August 10, 2023, Refined Sparse Capture Strategy.

Figure 3.16 Horizontal Views of the Resulting 3D Models. Scanning Date: August 10, 2023, Refined Sparse Capture Strategy.

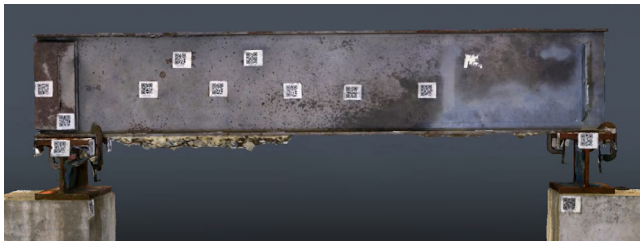

Figure 3.17 Vertical Views of the Resulting 3D Models. Scanning Date: August 10, 2023, Refined Sparse Capture Strategy.

During parameter validation, flight speed proved crucial for reliable data in confined spaces. The research team optimized drone structure to ensure thorough coverage while maintaining image fidelity. These ranges were confirmed through reference measurements and analyses of point cloud density and completeness.

The evolution of flight path strategies revealed best practices for drone-based data collection. The initial circular pattern (Iteration 1) caused connectivity gaps, while the multilevel approach (Iteration 2) resolved them but generated redundant data. The sparse capture strategy (Iteration 3) balanced coverage and efficiency by prioritizing strategic camera placement, reducing image counts and processing requirements while matching close-range photogrammetry reconstruction quality.

Key principles from laboratory testing will inform future standard protocols. Multilevel scanning paths with targeted edge capture provide comprehensive coverage. Camera parameter optimization, especially exposure and ISO settings, enhances model fidelity. Supplementary lighting is crucial for high-quality images in shadowed bridge areas. Systematic parameter optimization creates reliable and efficient drone-based inspection methodologies.

3.2.5 Field Implementation Strategies

Field testing in West Lafayette, Indiana, revealed challenges in drone-based bridge inspection beyond laboratory conditions. These insights helped adapt flight path planning for real-world scenarios.

The initial field deployment took place at Davis Ferry Road on September 11, 2023, and highlighted critical challenges in flight path execution. Using a DJI Matrice 300 equipped with a P1 camera, the research team captured 418 photos. However, losing RTK service and Global Navigation Satellite System (GNSS) signals beneath the bridge limited under bridge coverage to about 50% usable images. Figure 3.18 and Figure 3.19 illustrate the difficulty of maintaining complete coverage, emphasizing the importance of robust positioning methods when external GPS signals are compromised.

Figure 3.18 Summary of Field Implementation Testing Results at Davis Ferry Road Bridge. Target and Surroundings.

Figure 3.19 Summary of Field Implementation Testing Results at Davis Ferry Road Bridge. 3D Scanning Results.

Figure 3.20 Summary of Field Implementation Testing Results at S-Brite Bridge. Target and Surroundings.

A second field deployment at the S-Brite Bridge on November 13 and 16, 2023, improved reconstruction quality, especially in edge clarity and detail preservation. The revised scanning strategy included close-range detail captures and wider-angle overview shots, balancing high-resolution imaging with broader contextual coverage (Figure 3.20 and Figure 3.21). This dual distance strategy proved effective for handling repetitive steel girder features. Collecting approximately 3,000 images yielded notable gains in edge quality in well-lit areas.

Four key principles emerged from these field deployments:

- *Distance Management*: Varying the distance from the structure, combining close range captures for fine detail with wider angle shots for global context, proved crucial for reconstructing repetitive features in steel girder bridges.
- *Coverage Strategy*: Employing systematic overlap patterns while addressing site specific constraints is vital. Flight paths must be adaptable to environmental obstacles and access limitations yet maintain sufficient overlap for consistent image alignment.

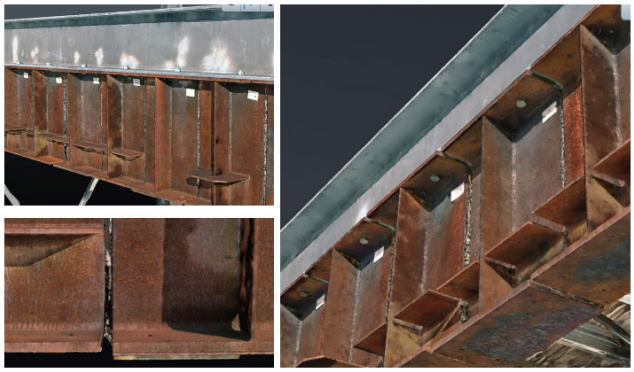

Figure 3.21 Summary of Field Implementation Testing Results at S-Brite Bridge. 3D Scanning Results.

- *Positioning Systems*: Reliable scanning strategies must be prepared for degraded GPS or RTK signals, particularly under bridge decks. Integrating visual positioning and carefully planning flight paths ensures the drone can maintain orientation when external signals are compromised.
- *Environmental Adaptation*: Adjusting flight paths based on lighting conditions plays a significant role in the quality of the final imagery. Capturing brighter areas first and using appropriate exposure settings for shadowed regions yielded more accurate edge details during reconstruction.

Collectively, these field implementations demonstrated that effective bridge inspection requires more sophisticated flight planning than laboratory tests alone might indicate. Balancing close range detail capture with broader contextual imaging, while adapting to site specific challenges, emerged as a key concern for optimal flight path design.

3.3 Field Implementation

Field implementation of 3D scanning for bridge inspection considers various environmental and site-specific factors affecting data quality and efficiency. This section examines three critical aspects: lighting conditions and exposure control, wind considerations, and site-specific access limitations. Strategies address these challenges, providing essential guidance for integrating 3D scanning into bridge inspection scenarios while ensuring data fidelity and operational safety.

3.3.1 Environmental Factors - Lighting Conditions and Exposure Control

Lighting conditions significantly impact photogrammetric reconstruction in bridge inspection. Preliminary tests at Bowen Laboratory confirmed the importance of managing lighting, but field implementation revealed complexities specific to bridge structures. Transitions between natural sunlight and shaded interior sections at girder webs and flanges create challenges.

Underexposed images in shadowed areas (Figure 3.22) can lead to incomplete or distorted regions in the final 3D model (Figure 3.23). Bridge inspections involve varying illumination, from exterior edges to deep shadows in the girder interior. This variation, especially at transition zones, can disrupt feature matching and reduce reconstruction quality.

Figure 3.22 Incorrect Exposure and Resulting Incomplete 3D Model Sections: Incorrect Exposure Picture.

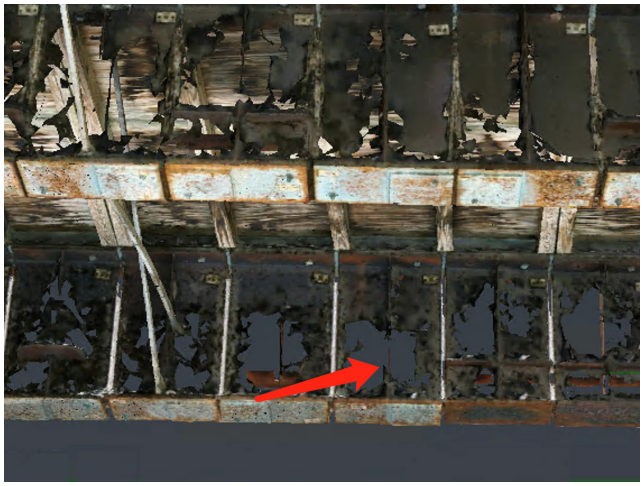

Figure 3.23 Incorrect Exposure and Resulting Incomplete 3D Model Sections: Lead Holes appearing in 3D Model.

The field tests evaluated exposure strategies in four distinct zones on a W-section specimen, each with unique lighting conditions. Figure 3.24 shows automatic and manual exposure controls. Automatic settings balanced scene brightness but underexposed shadows and overexposed edges. Manual control, using low ISO, controlled aperture, and consistent shutter speeds, produced higher completion rates in challenging regions. Below summarizes automatic and manual exposure testing.

- Automatic Exposure Testing:
  - Default camera settings attempting to balance overall scene brightness
  - Resulted in underexposed areas in shadow regions
  - Poor detail preservation in transition zones
  - Limited success in feature matching across varying light conditions

Figure 3.24 Exposure Settings in Different Zones.

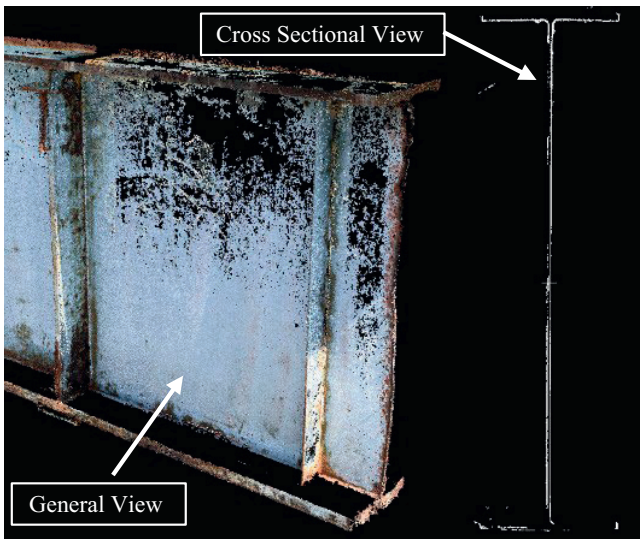

Figure 3.25 The Comparison of Model Construction Result (General and Cross-sectional Views). Auto-Exposure Model and Section Profile.

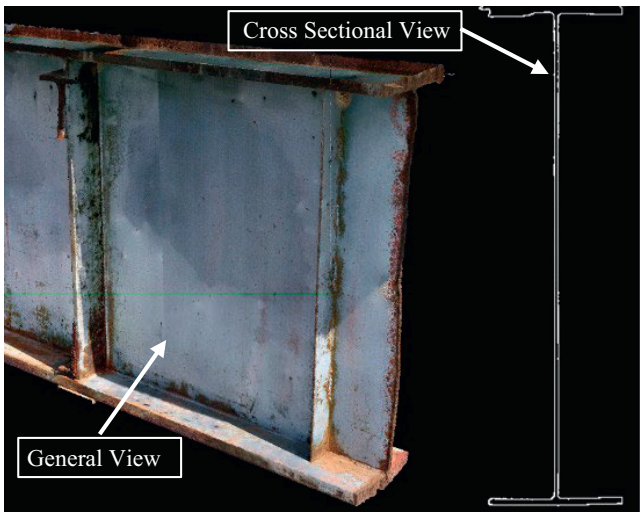

Figure 3.26 The Comparison of Model Construction Result (General and Cross-Sectional Views). Manual-Exposure Model and Section Profile.

- Manual Exposure Control (strategic adjustment of key parameters):
  - Low ISO settings to minimize noise
  - Controlled aperture for depth of field
  - Consistent shutter speed (1/200s) to prevent motion blur
  - Zone-specific exposure compensation
  - Graduated exposure adjustments in transition areas

Manual exposure control significantly improved the final reconstruction quality, especially in areas with severe contrast (Figure 3.25 and Figure 3.26). Handheld equipment validated these principles for drone-based inspection protocols, ensuring uniform image capture across lighting zones.

3.3.2 Environmental Factors: Wind Considerations

Wind conditions pose a significant challenge in bridge inspection due to the close-range flight required near structural elements. Even larger drone platforms like the DJI Matrice 300

RTK, with better wind resistance, experience unpredictable turbulence and channeling effects due to the proximity of bridge components.

During protocol development, the research team set conservative wind limits (26.84 mph) below manufacturer specifications to maintain data quality and safety near structures. Flight often occurs within 5–7 ft of girders, so sudden gusts can destabilize the drone or reduce image clarity.

3.3.3 Site-Specific Challenges Access Limitations

Access constraints hinder bridge inspection, especially capturing detailed steel girder geometry. Larger drones document exterior surfaces, but maneuvering within confined spaces is needed for web surfaces and bottom flanges. This prompted the research team to reevaluate equipment selection and scanning strategies.

Full-frame sensor drones deliver high-quality images but can be cumbersome in narrow gaps. The DJI Avata 2 was evaluated for its compact form factor and sensor performance. Smaller drones with wide-angle optics can successfully navigate interior W-sections and produce high-fidelity reconstructions, but image consistency varies under different lighting conditions.

Wide-angle optics (blue lines) in Figure 3.28 can distort, especially at frame edges. Calibration or correction algorithms are needed to preserve accurate feature matching and geometry in 3D models. Despite limitations, the DJI Avata 2 accessed tight interior sections and collected detailed images, filling coverage gaps larger aircraft could not. Key findings:

1. Navigation Capabilities:
   - Successfully maneuvered through limited spaces between W-sections
   - Demonstrated ability to maintain stable flight in confined conditions
   - Required careful speed control for optimal image quality
2. Data Quality:
   - Achieved significant improvement in web surface documentation
   - Successfully reconstructed inner surface details previously inaccessible
   - Maintained consistent image quality despite space constraints

Figure 3.27 Wide-Angle Image from Compact Drone.

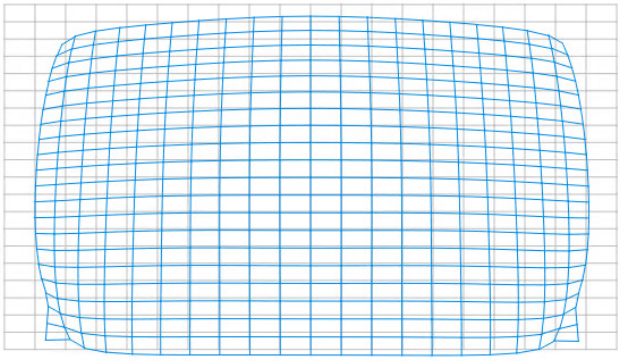

Figure 3.28 Strong Distortion from Wide-Angle.

Figure 3.29 Compact Drone Scanning Result: 3D Reconstruction Result.

3. Integration Strategy: The testing revealed the potential for a dual-platform approach:
   - Large drones (e.g., Matrice 300) for exterior and accessible areas
   - Compact drones (Avata 2) for confined spaces between girders
   - Data fusion between platforms for complete structural documentation

Field trials with the DJI Avata 2 successfully navigated confined spaces and captured 4K footage, reconstructing previously unreachable inner web surfaces (Figure 3.29 and Figure 3.30). Smaller drones sacrifice image quality but are essential for complete structural documentation. Integrating large and small drone platforms offers a dual approach: using larger drones for exterior surfaces and smaller units for tight spaces between girders, then merging data for a comprehensive representation.

Real-world operations require nuanced flight planning and specialized methods beyond laboratory work. Exposure optimization through manual control, conservative wind thresholds, and selective use of compact drones for confined areas ensure safe and high-quality data collection. By applying these measures, bridge inspection teams can effectively navigate on-site 3D scanning challenges, resulting in robust and accurate results.

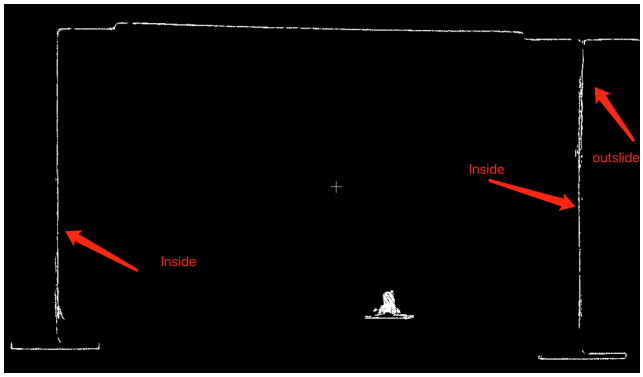

Figure 3.30 Compact Drone Scanning Result: More Complete Inner Section Profile.

3.4 Quality Control

Extensive experimental work at both laboratories and field sites revealed that successful 3D reconstruction of bridge structures depends on preliminary quality assessment procedures. Initial scanning attempts failed to provide sufficient feature points for photogrammetric reconstruction, especially on coated or polished steel surfaces. A preflight feature detection protocol improved scanning efficiency and reliability.

A real-time feature point detection system using Scale-Invariant Feature Transform (SIFT) algorithms is the cornerstone of this prescanning protocol. It operates during preliminary drone flyovers to assess surface feature detectability before full scanning. The feature detection software provides a comprehensive visualization of feature point distribution, including a heat map showing feature density and accumulated points over multiple frames. This visualization helps identify challenging areas during photogrammetric reconstruction.

Integration of exposure analysis tools within the prescanning workflow addresses challenging lighting conditions in bridge environments. Real-time exposure histogram analysis and image clarity metrics provide objective image quality measures, overcoming limitations of on-screen visual assessment, especially in varying lighting conditions. This capability proved valuable during field testing, where screen visibility can be compromised by strong ambient light or low illumination.

The feature detection interface (Figure 3.31) provides real-time feedback through a multiwindow display showing the original image, detected feature points, and corresponding exposure histogram. Operators can quickly identify problematic areas and adjust scanning parameters. The system implements automated thresholds for feature density, triggering warnings when features fall below levels required for reliable reconstruction.

Systematic comparison between feature detection results and final reconstruction quality validated the effectiveness of this prescanning protocol. Data from multiple scanning sessions showed a strong correlation between preliminary feature point density measurements and successful 3D model reconstruction. This correlation allows reliable prediction of scanning feasibility and optimal resource allocation for bridge documentation.

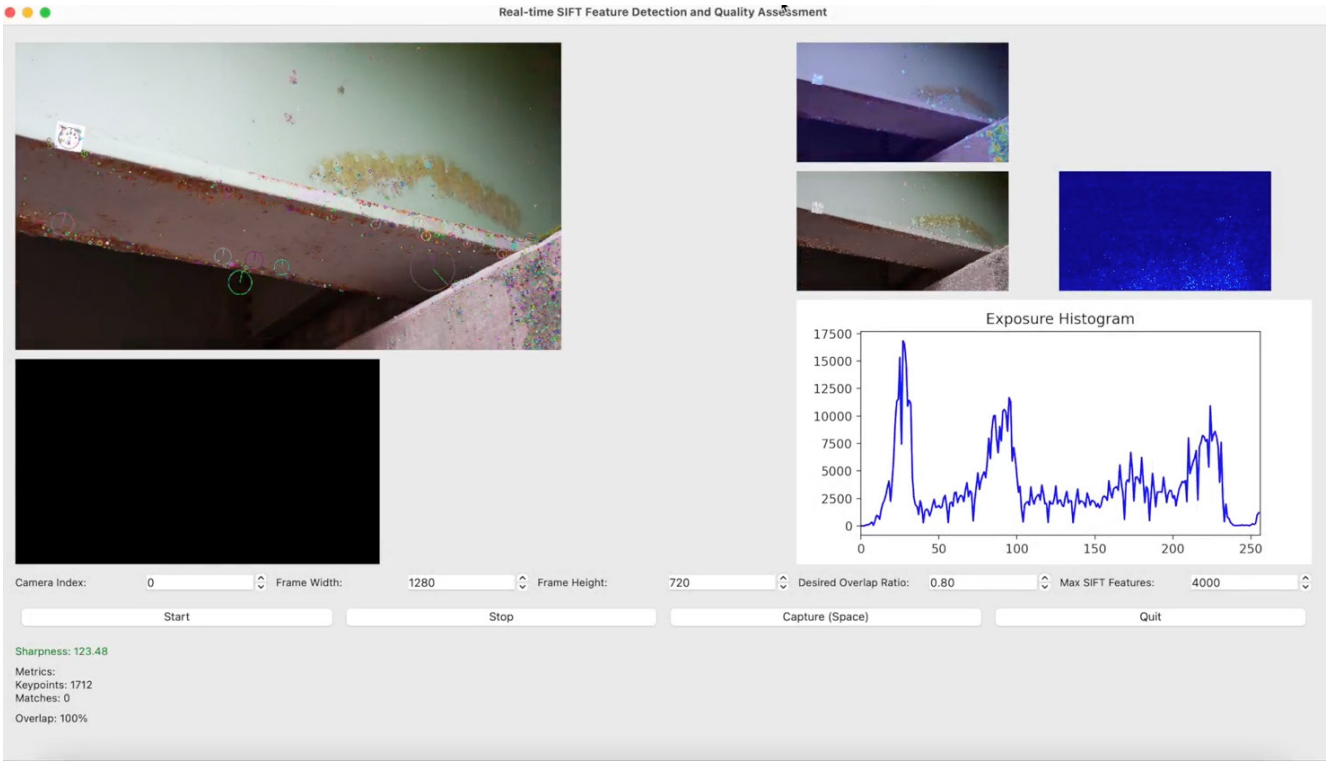

Figure 3.31 Screenshot of Feature Detection Interface Showing Multiple Windows With Original Image, Feature Detection Results, and Exposure Histogram.

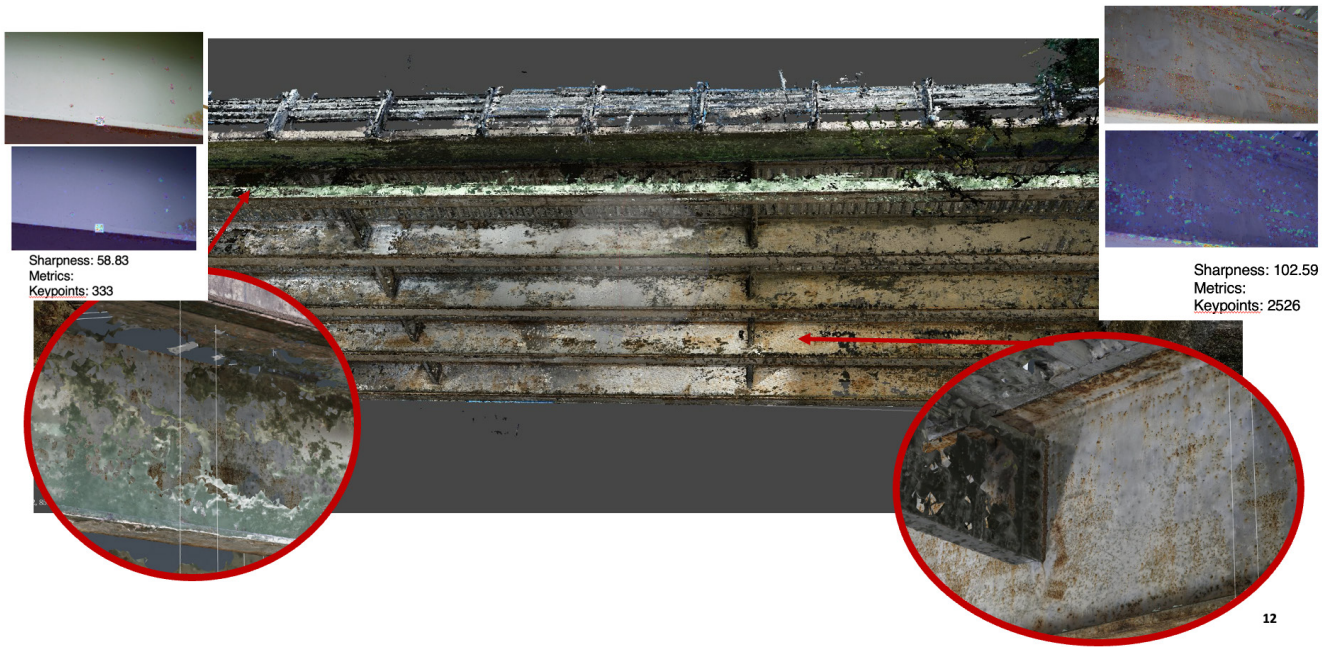

Figure 3.32 The Comparison of Feature Points Number to the Quality of Model in Different Place of The Bridge.

This prescanning quality check protocol significantly improves bridge scanning efficiency. It identifies potential reconstruction challenges before full scanning, preventing resource-intensive data collection for unsuitable results. This approach is especially valuable for complex bridge structures with varying surface conditions.

3.5 Lessons Learned and Best Practices

Extensive field implementation and testing by the research team led to comprehensive insights into effective 3D scanning practices for bridge inspection. This section presents two case studies illustrating practical scanning protocol refinement. The first case study at the Davis Ferry Road Bridge showcased optimized strategies, while the second case study integrated multiple platforms for complete bridge documentation, highlighting complementary technology strengths and operational considerations. These real-world implementations demonstrate successful scanning strategies and critical factors for future bridge inspection.

3.5.1 Practice 1: Implementation of Optimized Scanning Strategy at Davis Ferry Road Bridge

Field implementation at the Davis Ferry Road Bridge (1000–1067 Davis Ferry Rd, West Lafayette, IN 47906) in April 2024 offered insights into practical challenges and optimization strategies for bridge scanning (Figure 3.33). Wind conditions (maximum recorded wind speeds of 13.7 m/s) necessitated two sessions (April 17 and 25, 2024), emphasizing environmental considerations in scanning operations.

The research team developed a comprehensive scanning strategy with multiple elevation layers to cover the bridge structure. The scanning path focused on capturing detailed data from two W-sections, varying camera angles and exposure settings for maximum data quality. The multilayer approach effectively captured the bridge's complex geometries, especially the underside details through optimized camera angles (Figure 3.34).

The implementation revealed critical findings about surface characteristics and their impact on photogrammetric reconstruction. External web surfaces, despite adequate illumination, posed challenges due to their smooth, patternless surface, leading to suboptimal feature detection. Interior web surfaces, with lower illumination, showed better reconstruction quality, suggesting surface texture is more crucial than lighting alone.

Key improvements implemented during this field operation included:

- Developing manual exposure control strategies that adapt to different surface conditions.
- Enhancing the scanning angle coverage to ensure comprehensive data capture.
- Increasing the overlap between adjacent images to improve the reconstruction process.
- Modifying the camera positioning to capture the intricate details of the bridge structure.

Despite achieving comprehensive coverage and optimized scanning, certain W-section components' smooth surfaces posed challenges for feature detection and reconstruction. Further research is needed on surface feature enhancement methods and alternative scanning strategies for highly polished or uniform surfaces.

Figure 3.33 Details of Scanning Location, Overview Picture and Locations from Satellite Map (Map Data: ©2016, 2025 Google).

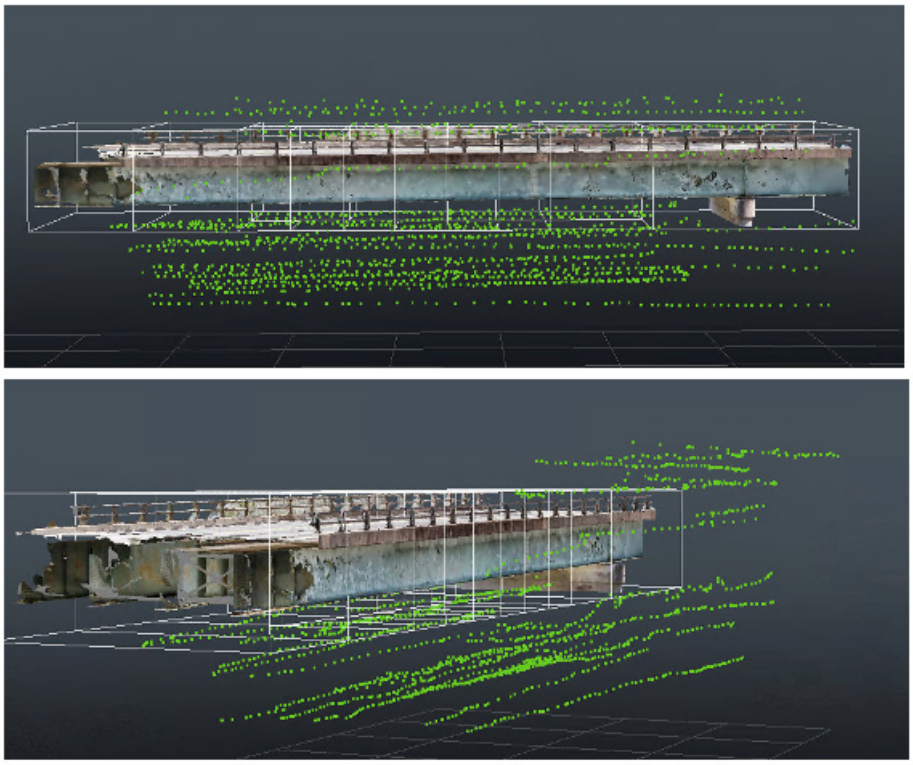

Figure 3.34 Visualization of the Scanning Path Showing a Profile View (Top) and an Isometric View (Bottom) to Demonstrate Multiple Elevation Layers and Comprehensive Coverage.

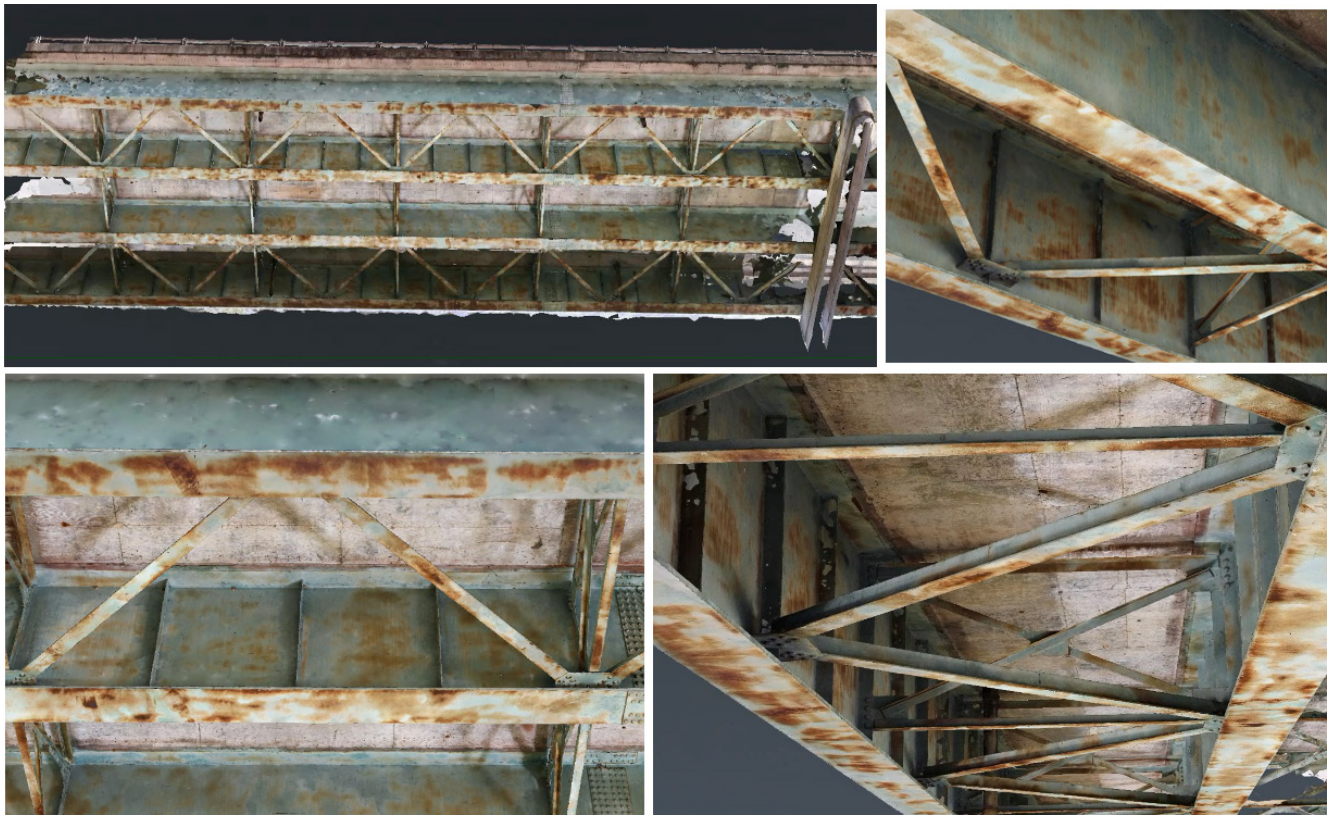

Figure 3.35 High-Fidelity 3D Reconstruction of the Davis Ferry Road Bridge Showing Detailed Capture of Structural Elements and Surface Features.

The scanning implementation achieved remarkable results in model reconstruction quality, as shown in Figure 3.35. The reconstructed model exhibits exceptional detail and geometric accuracy, especially in capturing the bridge's complex structural elements. This level of quality represents a significant advancement in field scanning capabilities, showcasing the effectiveness of the optimized scanning methodology.

The exceptional visual quality of the reconstruction validates the effectiveness of the implemented scanning strategies, particularly the multilayer approach and optimized exposure settings. This success in field conditions shows that high-quality photogrammetric reconstruction of bridge structures is achievable with proper protocols, despite varying surface conditions and environmental factors. Insights from this implementation inform refinements in scanning methodology, aiming to replicate this quality across diverse bridge structures and environments.

3.5.2 Practice 2: Multiplatform Integration for Complete Bridge Documentation

The research team integrated multiple scanning platforms to achieve comprehensive 3D bridge documentation. Three data collection methods were used: a DJI Matrice 300 RTK for main structural elements, a DJI Avata 2 for confined spaces, and handheld cameras for bottom-view documentation. The RTK system provided accurate geometric reconstruction with scaling constraints.

The integration of point clouds from various sources created a comprehensive bridge model encompassing the superstructure, deck, and W-sections (Figure 3.36). Visualizing the point cloud reveals distinct characteristics from each scanning platform, reflecting the data collection method's capabilities and limitations.

The implementation revealed significant operational considerations. Despite not achieving complete vertical coverage, the scanning operation required more than eight hours of field work, emphasizing the importance of battery management. Maintaining a complete battery set ensured continuous operation and adequate redundancy for safety. Proper battery cooling periods were also necessary to prevent equipment degradation.

The integrated point cloud model achieved remarkable reconstruction quality, capturing intricate structural details like the bridge's superstructure, deck surface conditions, and supporting elements (Figure 3.37). The high-fidelity color reproduction and clear definition of structural components showcase the effectiveness of the multiplatform approach in capturing comprehensive bridge documentation.

Analysis of confidence metrics from different scanning platforms revealed distinct quality patterns (Figure 3.37). The DJI

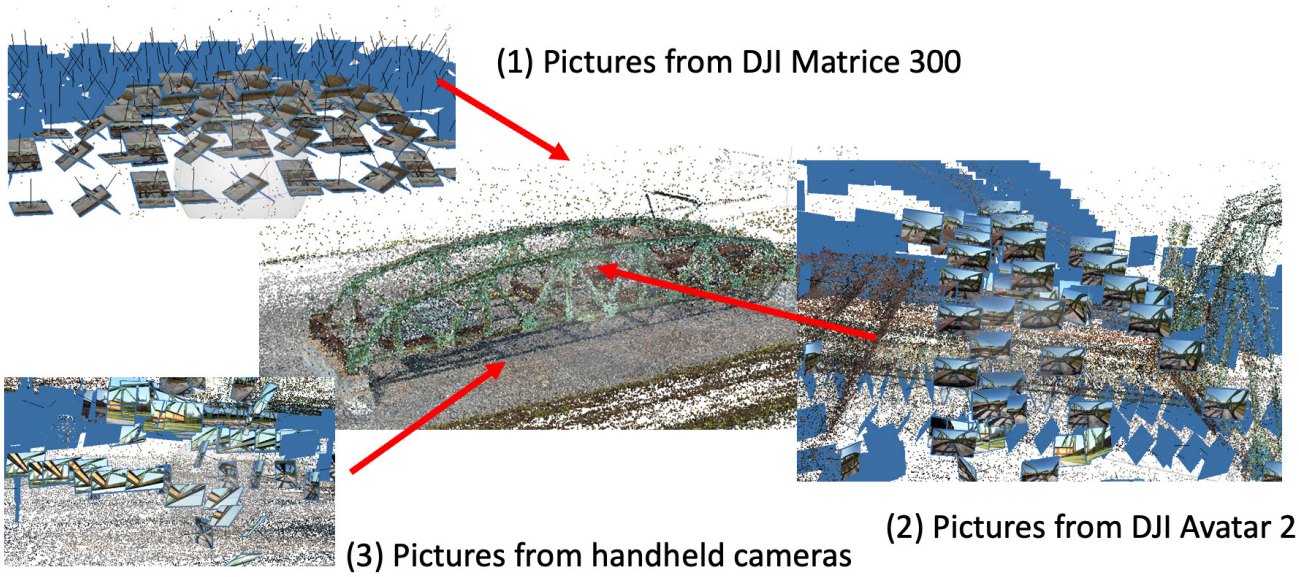

Figure 3.36 Integrated Point Cloud Visualization Showing Contributions From Multiple Scanning Platforms. Different Colors Indicating Data Sources: DJI Matrice 300 (Source 1), DJI Avata 2 (Source 2), And Handheld Cameras (Source 3).

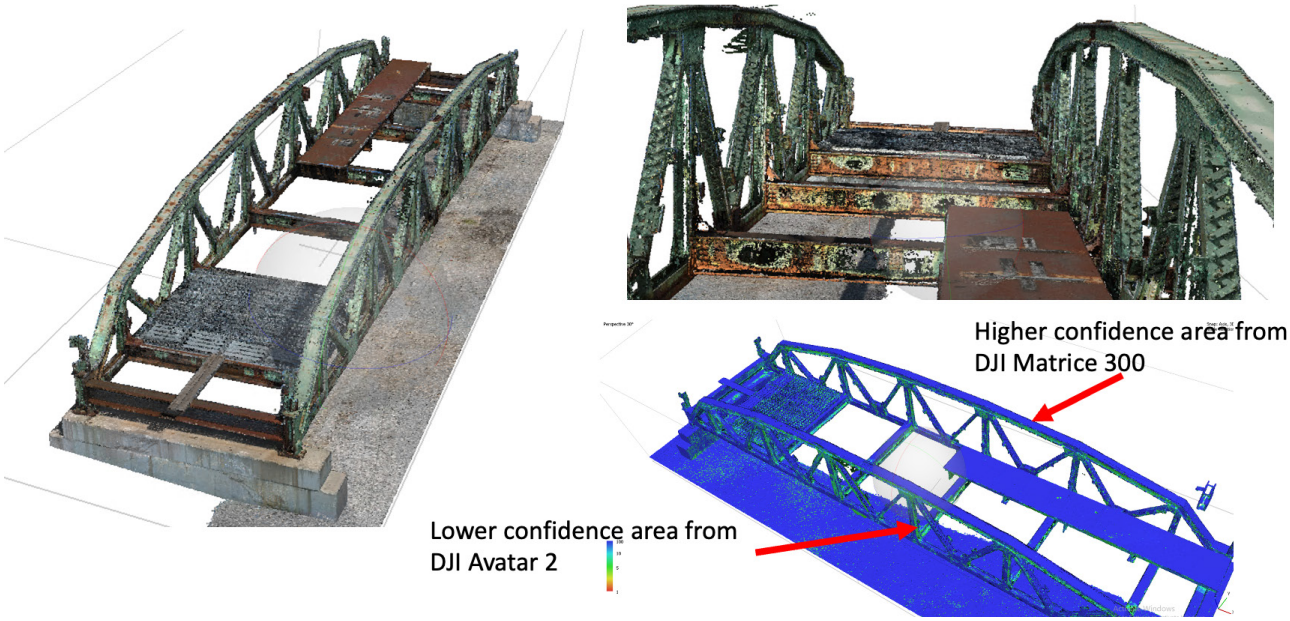

Figure 3.37 High-quality 3D Reconstruction Showing Overall Bridge Structure With Detailed Texture and Geometric Capture and Confidence Analysis Visualization Showing Varying Quality Levels From Different Scanning Platforms.

Matrice 300's full-frame sensor consistently produced higher confidence in reconstruction, especially in upper structural elements and exposed surfaces. The DJI Avata 2, while useful for confined spaces, generated lower confidence metrics. This variation guides filtering and optimizing the final model, ensuring selective use of high-confidence data from each platform for optimal reconstruction.

This implementation suggests multiple scanning platforms for comprehensive bridge documentation, but operational efficiency must be considered. For future small drone use in confined spaces, the research team recommends balancing image capture and video recording. Image-based reconstruction offers better quality, but video recording may be more time-efficient for limited coverage within short operational windows.

3.6 Summary of the Chapter

The development of 3D scanning protocols for bridge inspection revealed critical findings impacting photogrammetric reconstruction in field conditions. Systematic investigation of prescanning quality assessment and multiple field implementations identified key factors influencing scanning success and strategies for reliable results.

Prescanning quality assessment, particularly real-time feature point detection using SIFT algorithms, predicted reconstruction feasibility before full scanning. This approach was especially valuable for polished steel surfaces where traditional visual assessment might fail. Exposure analysis tools and automated quality metrics provided objective measures for scanning feasibility, enhancing efficiency.

Field implementation at the Davis Ferry Road Bridge demonstrated the importance of comprehensive scanning strategies and environmental considerations. Surface characteristics significantly impacted reconstruction quality. Exterior web surfaces with smooth, patternless characteristics posed challenges despite adequate illumination, while interior surfaces showed better reconstruction potential despite lower light. These findings highlight the complex relationship between surface texture, lighting, and reconstruction success.

The multiplatform integration approach revealed the potential and limitations of current scanning technologies. Combining large drones (DJI Matrice 300), compact drones (DJI Avata 2), and handheld cameras showed that comprehensive bridge documentation requires a strategic mix of platforms. Each platform had advantages: the Matrice 300's full-frame sensor provided superior image quality for accessible areas, while the Avata 2 was essential for confined spaces. The integration achieved more complete documentation than any single platform.

Operational considerations were crucial. Extended scanning operations exceeded eight hours, highlighting the importance of battery management and redundancy. Environmental factors, especially wind, impacted scanning feasibility and data quality, necessitating careful weather planning.

These findings provide the basis for standardized bridge inspection protocols using 3D scanning. Controlled testing and field implementation demonstrated that successful documentation requires a systematic approach considering technical capabilities, environmental conditions, and operational constraints. These lessons inform comprehensive guidelines for implementing 3D scanning in routine bridge inspection.

4. GUIDELINE AND RECOMMENDATION FOR 3D BRIDGE SCANNING

A well-structured guideline is essential for successful 3D scanning of bridges. Modern bridge inspections require sophisticated methods to capture and document structural conditions, especially for detecting deterioration in critical elements. Extensive laboratory testing and field implementations in Indiana have developed comprehensive protocols for routine bridge inspections using 3D scanning.

This section provides practical guidelines for selecting, deploying, and managing 3D scanning technologies in bridge assessments. Systematic evaluation revealed that successful bridge documentation requires careful consideration of environmental conditions, equipment capabilities, and operational constraints. These guidelines address critical aspects of implementation, from technology selection to data processing and management, ensuring transportation agencies effectively integrate advanced tools into their inspection programs.

The workflow outlined in Figure 4.1 systematically implements 3D scanning for bridge inspection. It involves selecting technology based on requirements and site conditions, field preparation, execution, data processing, and management. Each phase ensures reliable and efficient data collection.

Optimized for steel girder inspection in Indiana, the process emphasizes critical decision points and quality control. Detailed guidelines and recommendations follow, based on research and practical experience.

4.1 Selection of 3D Scanning Technologies

The selection of appropriate scanning technology is crucial for successful bridge inspection. Modern bridge inspection requires sophisticated methods to capture structural conditions accurately and efficiently. Traditional visual inspection remains important, but advanced 3D scanning has revolutionized bridge documentation and assessment. Factors like accuracy, accessibility, and operational efficiency must be carefully balanced when choosing technology.

Recent advancements in UAV technology have revolutionized bridge inspection. UAVs provide unprecedented access to challenging areas, enabling comprehensive documentation of bridge conditions. Their rapid coverage of large areas makes them a preferred choice for initial assessments and routine inspections.

CRP complements UAVs by capturing fine surface details and creating high-resolution 3D models. Its cost-effectiveness and portability make it valuable for focused inspections.

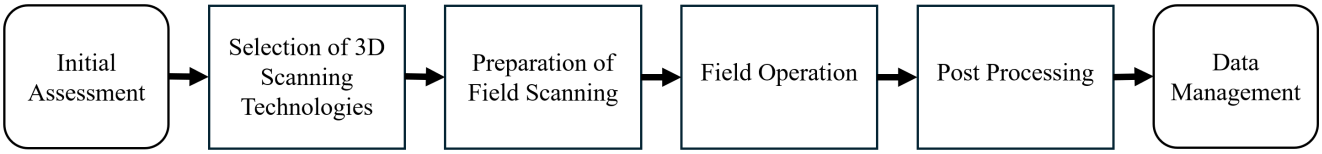

Figure 4.1 Guideline for 3D Bridge Scanning.

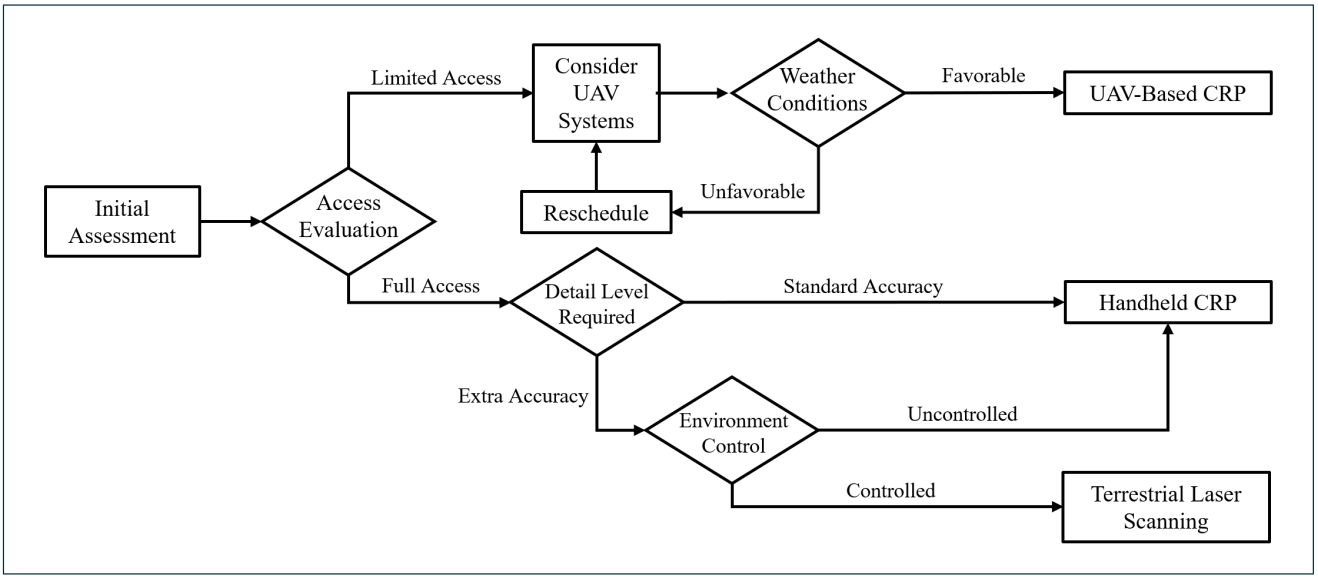

Figure 4.2 Selection Flow for 3D Scanning Method.

TLS offers high precision but faces operational challenges in field conditions. Stable setup positions, clear lines of sight, and controlled environments limit its practical application. However, TLS remains valuable for specific applications requiring extremely high precision and site conditions permitting proper setup.

Selection workflow for 3D scanning methods to guide inspectors in choosing the best scanning technology is shown in Figure 4.2. It considers factors like accessibility, accuracy, and environmental conditions identified through research at Bowen Laboratory and field bridge sites.

The decision workflow involves systematic evaluation of scanning technologies under varying conditions. Controlled laboratory experiments and field implementations at multiple bridge sites in Indiana revealed that technology selection should consider three primary factors: required measurement accuracy, site accessibility, and environmental conditions. Quantitative performance evaluations and practical implementation experiences led to these recommendations.

- UAV-based and Handheld CRP
  - Optimal for comprehensive bridge documentation
  - Best for both overall bridge inspection and detailed surface documentation
  - UAV excellent for accessing difficult areas under bridge and between girders
  - Handheld ideal for precise measurements and defect mapping
  - Quick setup and data collection with immediate quality checks
  - Works best in overcast to bright daylight, avoid direct sunlight
  - Requires clear weather with wind under 15 mph for UAV operations
  - Cost-effective with standard camera equipment
  - FAA certification needed for UAV, basic training for handheld
  - Can combine both methods for complete bridge coverage
- TLS
  - Highest precision (±0.003–0.005in at 33 ft range)
  - Ideal for specialized high-precision measurements
  - Generates immediate PCD
  - Requires stable ground conditions for setup
  - Takes longer to set up but highly reliable
  - Higher equipment cost than photogrammetry
  - Best suited for bridges with good access points
  - Limited by line-of-sight to bridge elements
  - Professional training required for operation
  - Most effective in controlled environments

Thorough preparation for field implementation becomes critical after selecting the appropriate scanning technology using the decision workflow. Successful scanning operations require careful consideration of prescanning assessments, environmental conditions, and operational protocols detailed in the following section.

4.2 Preparation of Field Scanning

Successful 3D scanning of bridge structures requires thorough preparation and careful planning. This preparatory phase ensures efficient data collection and high-quality results. Planning considers technical requirements, safety, environmental conditions, and regulatory compliance, especially for UAV operations (see Preoperation Checklist in Table 4.1).

The Preoperation Checklist (Table 4.1) sets the stage for successful field scanning. With proper preparation, teams can proceed to field operations, where these carefully planned procedures are implemented. This section details the systematic approach required during active scanning, ensuring high-quality data collection.

TABLE 4.1
Preoperation Checklist.

CHECK	ITEMS
	Verify environmental conditions: • No precipitation • Proper lighting conditions (overcast to bright daylight, avoid direct sun)[1] • Wind speed below 15 mph for UAV operations[2]
	Complete equipment readiness check: • All batteries fully charged • Memory cards formatted • Lens/sensors cleaned • Backup power supplies prepared
	Configure camera settings: • ISO: 100-400 for optimal noise control • Shutter speed: minimum 1/200s for UAV • Aperture: f/4.0-f/5.6 for depth of field [3]
	Verify UAV systems: • Gimbal operation and calibration • RTK signal reception • Obstacle avoidance systems • Controller firmware updated
	Review flight compliance: • Check airspace restrictions • Verify FAA authorization • Contact local air traffic control if required
	Prepare scanning strategy: • Flight paths planned and loaded • Coverage patterns verified • Alternative landing zones identified
	Safety equipment check: • High-visibility vests • Safety barriers if needed • First aid kit • Communication devices

[1] Lighting Conditions: Field testing has established optimal scanning conditions under different scenarios:
- *Best: Overcast days (uniform, diffused light)*
- *Good: Early morning/late afternoon (indirect sunlight)*
- *Acceptable: Bright daylight with minimal shadows*
- *Avoid: Direct midday sun, heavy cloud cover, or dawn/dusk*

These conditions correspond to technical illumination ranges (2,000–20,000 lux) validated through extensive field testing at multiple bridge sites. Laboratory studies at Bowen Laboratory demonstrated that consistent, diffused lighting produces the most reliable photogrammetric reconstructions of steel girders.

[2] Wind Speed Thresholds: Based on comprehensive field implementation studies:
- *Optimal: < 10 mph (stable flight, best data quality)*
- *Acceptable: 10–15 mph (increased precautions required)*
  - *Reduce flight speed*
  - *Increase image overlap*
  - *Monitor battery consumption*
- *Restricted: > 15 mph (suspend operations)*

These thresholds ensure both data quality and operational safety, particularly critical for under-bridge scanning operations.

[3] Camera Settings: Through systematic testing at Davis Ferry Road Bridge, optimal camera parameters for steel girder inspection were identified:
- *ISO: 100-400 (minimizes noise in shadow areas)*
- *Shutter Speed: Minimum 1/200s (prevents motion blur during UAV operations)*
- *Aperture: f/4.0-f/5.6 (balances depth of field with light gathering)*
- *Focus: Manual focus preferred, with focus distance set to anticipated scanning range*

These settings provided optimal results for feature detection and model reconstruction quality across various bridge conditions.

4.3 Field Operation

The checklist and guidelines establish the foundation for successful field scanning. With proper preparation, teams can proceed to field operations, where these procedures are put into action. This section details the systematic approach during active scanning. More details are provided in Appendix A.

TABLE 4.2
Field Operation Checklist.

CHECK	ITEMS
	UAV-Based Close-Range Photogrammetry Checklist
	Preflight Check: • Check propeller condition and sound[1] • Turn on all safety features[2] • Check GPS connection[3]
	During Flight: • Watch battery level[4] • Monitor image coverage[5] • Check image quality regularly[6] • Maintain steady flight path[7]
	Handheld Close-Range Photogrammetry Checklist
	Camera Setup: • Check camera settings [8] • Check lighting conditions[9] • Prepare scanning path[10]
	Manual Operation: • Keep steady scanning distance[11] • Maintain image overlap[12] • Follow planned pattern • Review captured images

[1] Propeller System Diagnostics: Normal operation produces a consistent 5800±200 RPM sound signature. Any asymmetric sound patterns or frequency variations indicate potential mechanical issues requiring immediate system check. Critical for both flight safety and data quality.

[2] Safety Systems Protocol: Includes RTK positioning system (accuracy ±0.8in), obstacle avoidance sensors (effective range 1.6–98 ft), and redundant control systems. All systems must be verified through preflight diagnostic checks.

[3] GNSS Signal Quality: Minimum 7 satellites for RTK fixed solution. PDOP value should remain below 3.0 for optimal positioning accuracy. Monitor both horizontal and vertical dilution of precision.

[4] Power Management Protocol: Maintain 20% minimum reserve capacity (approximately 10 min flight time for M300 RTK). Monitor cell voltage differential (maximum 0.3V variance) and pack temperature (optimal range 68–95 °F).

[5] Coverage Parameters: Maintain 75% forward overlap and 65% side overlap for optimal photogrammetric reconstruction. Maximum ground sampling distance of 0.4 in./pixel at typical inspection range.

[6] Image Quality Metrics: Monitor exposure histogram for balanced distribution, maintain focus consistency (> 90% focus score), and verify motion blur index remains below 0.3.

[7] Flight Path Stability: Maintain consistent altitude ±3.3 ft, speed within 4.5–11 mph range, and gimbal stability within ±0.02° for optimal image quality.

[8] Camera Configuration: For optimal results, maintain consistent settings throughout scanning:
- *ISO: 100–400 range for clean images*
- *Shutter: Minimum 1/200s for sharp capture*
- *Aperture: f/4.0-f/5.6 for good depth of field*
- *Focus: Manual mode preferred*

[9] Illumination Requirements: Optimal range 180–1850 ft-candles, with diffused lighting preferred. Monitor shadow contrast ratio (< 4:1) and avoid specular highlights (peak intensity < 90%).

[10] Scanning Pattern Optimization: Systematic coverage ensuring maximum incident angle < 30° to surface normal. Grid pattern with 60% minimum overlap between adjacent positions.

[11] Distance Control: Maintain consistent working distance within ±10% of planned range to ensure uniform ground sampling distance and depth of field coverage.

[12] Image Overlap Parameters: Minimum 60% overlap in both horizontal and vertical directions, ensuring at least 3 views per surface point for reliable photogrammetric reconstruction.

Successful field scanning requires careful coordination and constant attention to data quality. Extensive field testing showed that dividing complex structures into manageable sections ensures consistent coverage and quality. Regular monitoring of environmental conditions and equipment status ensures reliable data collection and operational safety.

Once field scanning is complete, systematic processing generates useful 3D models from collected data. Proper field operations and documentation significantly impact this processing. This section details essential steps, starting with initial data verification and ending with final model generation.

4.4 Postprocessing

The postprocessing phase transforms raw field data into usable 3D models using systematic workflows. Extensive testing with various bridge structures led to optimized procedures using industry-standard software (Agisoft Metashape and Bentley iTwin Modeler) for photogrammetric reconstruction.

The Post Processing Checklist (Table 4.3) bridges raw field data to actionable inspection results. Systematic testing at multiple bridge sites, including the Davis Ferry Road Bridge implementation, revealed that proper execution of these steps ensures reliable geometric reconstructions. The quality of final 3D models directly impacts their utility for structural assessment and long-term bridge management.

Successful postprocessing requires balancing processing parameters and computational resources. Field implementations show that a typical bridge inspection dataset expands from 5–15 GB of raw imagery to 50–100 GB of processed data, including point clouds, mesh models, and analysis results. This expansion necessitates careful storage and processing considerations. Higher quality settings yield better results, but practical constraints require optimizing parameters to achieve optimal outcomes within available resources.

The successful generation of accurate 3D models marks a milestone in bridge inspection workflow, but it also creates new challenges in data organization and storage. This section addresses these challenges with systematic data management protocols, ensuring accessible and usable raw data and processed results throughout the bridge inspection lifecycle.

4.5 Data Management

Effective data management is crucial throughout the bridge inspection process. We have developed comprehensive protocols ensuring data integrity, traceability, and usability. These address immediate operational needs and long-term archival requirements.

Properly executing data management protocols (Table 4.4) ensures bridge inspection data remains accessible and usable throughout its lifecycle. Systematic data management is crucial for immediate inspection needs and long-term bridge monitoring and analysis. Organized storage and documentation of raw data and processed models support structural analysis, condition assessment, and decision-making.

This comprehensive guideline establishes a robust foundation for advanced bridge inspection using 3D scanning technologies.

TABLE 4.3
Post Processing Checklist.

CHECK	ITEMS
	Data Preparation: • Verify all raw files are complete[1] • Create working backup copies[2] • Check computer capability[3] Initial Processing: • Extract image features[4] • Align photo positions[5] • Optimize camera alignment[6] Model Generation: • Build dense point cloud[7] • Check point cloud quality[8] • Adjust model scale[9] Final Steps: • Export inspection products[10] • Generate process report[11] • Archive project files[12]

[1] Data Verification: Compare field collection logs with raw files. Typical dataset includes 300–1000 images per bridge section, requiring 5–15 GB storage.

[2] Backup Protocol: Create minimum two copies on separate storage devices. Original raw data must remain untouched throughout processing.

[3] System Requirements: Minimum 32 GB RAM for standard processing. GPU with 8 GB VRAM recommended. Storage requirements typically increase 10-15x during processing. Professional 3D reconstruction software (Agisoft Metashape / iTwin Capture Modeler) is required to complete upcoming steps.

[4] Feature Extraction (Agisoft Metashape):
- *Quality setting: High*
- *Key point limit: 40,000*
- *Tie point limit: 4,000*
- *Typically requires 1–2 hr for 500 images.*

[5] Alignment Parameters:
- *Accuracy: High*
- *Reference preselection: enabled*
- *Key point limit: 40,000*
- *Expected alignment rate > 95% for proper field capture.*

[6] Camera Optimization:
- *Parameters: f, cx, cy, k1-k4, p1, p2*
- *Optimization error threshold: 0.5 pixels*
- *Targets sub-pixel accuracy for control points.*

[7] Dense Cloud Generation:
- *Quality: High/Medium based on computer capability*
- *Depth filtering: Aggressive*
- *Typical point density: 0.1–0.2 in. point spacing*

[8] Quality Control:
- *Coverage completeness > 98%*
- *Noise level < 0.04in at 15 ft range*
- *Check for artifacts and gaps*
- *Consider subsampling if point cloud exceeds 100M points.*

[9] Scale Adjustment:
- *Use known control distances*
- *Verify global accuracy (target: ±0.2in at 15 ft)*
- *Check local accuracy (target: ±0.04in at 3 ft)*

[10] Export Formats:
- *E57/LAS for point clouds*
- *OBJ/FBX for mesh models*
- *Consider octree structure for large datasets*

[11] Documentation:
- *Processing parameters*
- *Quality metrics*
- *Time stamps*
- *Software versions*

[12] Archival Requirements:
- *Raw images: Original format*
- *Project files: Agisoft Metashape / iTwin Capture Modeler native formats*
- *Processed results: Standard formats*
- *Reports: PDF documentation*
- *Typical project size: 50–100GB total.*

TABLE 4.4
Data Management Checklist.

CHECK	ITEMS
	During Field Operations
	Back up your data every 30 min[1]
	Name files clearly with date and location[2]
	Watch your storage space[3]
	Record field conditions[4]
	Postoperation Tasks
	Move data to secure storage[5]
	Check data quality and completeness[6]
	Organize all project files[7]
	Create final delivery package[8]
	Update project documentation[9]

[1] Backup Protocol: Create incremental backups during field operations. Maintain minimum two separate storage devices with checksum validation. Typical field session requires 15–30 GB storage capacity with redundancy.

[2] File Naming Standard: Format: "BRIDGEID_DATE_SECTION_OPERATOR." Include essential metadata for database integration and project tracking. Critical for maintaining systematic data organization.

[3] Storage Requirements: Monitor real-time storage usage. Maintain minimum 25% free space on capture devices. Field operations typically generate 5–15 GB/hr of raw data depending on scanning parameters.

[4] Field Documentation: Record environmental conditions, equipment configurations, and scanning positions. Essential for quality assessment and processing optimization.

[5] Data Transfer Specifications: Implement verified transfer protocols with integrity checking. Typical project structure requires 100–150 GB total storage, distributed across processing and archival systems.

[6] Quality Control Parameters:
- *Image integrity: Focus quality > 90%*
- *Coverage verification: Minimum 60% overlap*
- *Dataset completeness: > 98% target coverage*
- *Data validation: Checksum verification*

[7] Project Organization Structure:
- *Raw data: Original capture files*
- *Processing: Software-specific project files*
- *Products: Point clouds and models*
- *Documentation: Technical reports and metadata*

[8] Deliverable Requirements:
- *Point clouds: E57/LAS format, indexed*
- *Project files: Native software formats*
- *Reports: PDF with embedded metadata*
- *Storage media: Enterprise-grade devices*

[9] Documentation Standards:
- *Processing parameters*
- *Quality metrics and validation results*
- *Field operation records*
- *Project metadata and version control*
- *Bridge management system integration data*

Systematic data collection, processing, and management ensure high-quality geometric data for structural assessment. Proper data collection and management serve as the groundwork for advanced structural analysis and decision-making. The following framework section converts PCD into meaningful structural assessments, enabling efficient bridge condition evaluation and informed maintenance decisions without complex finite element modeling.

5. FRAMEWORK FOR BRIDGE INSPECTION UTILIZING 3D SCANNING

The proposed framework utilizes advanced 3D scanning technologies to analyze the residual strength of bridge components. This offers an alternative to traditional FEA approaches. By converting raw PCD into actionable structural assessments, this framework allows transportation agencies to make efficient decisions regarding bridge maintenance and repair priorities. The framework balances speed and precision, serving as a non-FEA solution for most cases while clearly distinguishing scenarios requiring detailed FEM analysis, such as severe section loss, complex load interactions, or critical infrastructure evaluations.

The framework operates through a structured sequence of modules, designed to systematically assess bridge conditions with minimal computational overhead. it consists of three core modules: (1) deterioration analysis, (2) residual strength evaluation using empirical equation, and (3) residual capacity evaluation through traditional FEA.

1. Deterioration analysis assesses corroded steel girders for material loss, thickness reduction, and damage distribution on webs. to evaluate their residual strength and structural integrity.
2. Residual strength estimation uses empirical equations (from Kanakamedala et al.'s (2023) SPR-4527 project) to estimate the remaining load-carrying capacity of corroded steel girders based on predefined mathematical models, considering factors like section loss, crippling capacity, and material properties.
3. Residual capacity evaluation through FEA simulates the structural behavior of corroded steel girders under load, providing a detailed assessment of stress distribution, deformation and ultimate strength.

The first and second modules are essential to implement, and the third module is recommended when empirical equation-based estimates are inadequate or needed to validate empirical predictions and support maintenance decisions by assessing ultimate load-carrying capacity. The overall framework workflow is shown in Figure 5.1.

This chapter explains each module in detail. The research team implemented a case study using this proposed framework. The results of the case study are followed by a discussion of the three modules.

5.1 Deterioration Analysis Using Point Cloud Model

Deterioration analysis in this framework uses high-resolution PCD to characterize corrosion in steel girders. It processes 3D scans of the girder's surfaces to calculate localized thickness values and pinpoint areas of section loss or other defects. These outputs provide a high-resolution map of current structural conditions for accurate residual strength assessments. The following subsections explain how web thickness is measured using a grid-based approach and how damage areas are identified, emphasizing precision and manageable data processing.

5.1.1 Web Thickness Measurement

This subsection explains how the framework determines local thickness values from raw PCD for consistent thickness measurements across scanning technologies. It converts the original text-based PCD to a comma-separated values (CSV) file, establishes a global coordinate system, and defines a grid to systematically sample the girder's web. Figure 5.2 shows steps of thickness measurement.

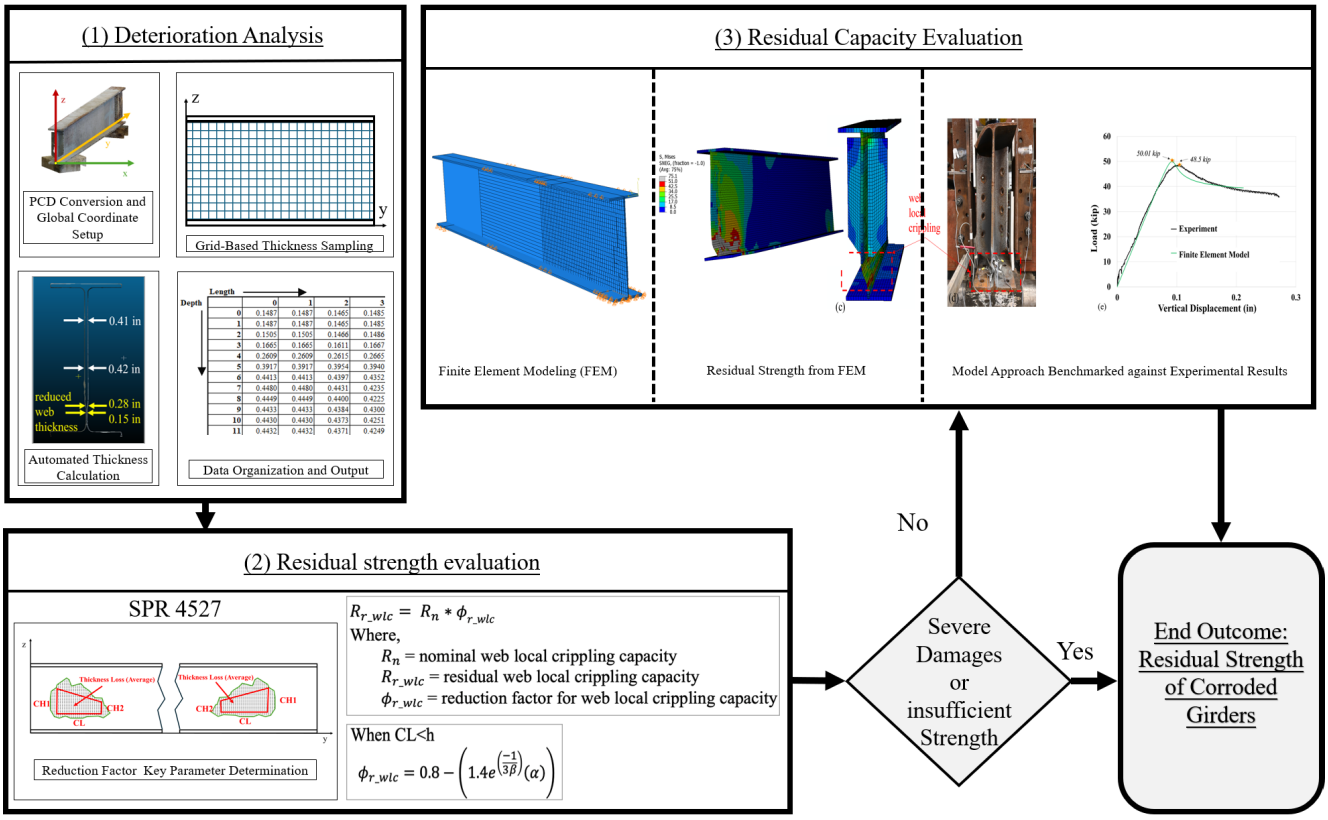

Figure 5.1 Overall Framework Workflow.

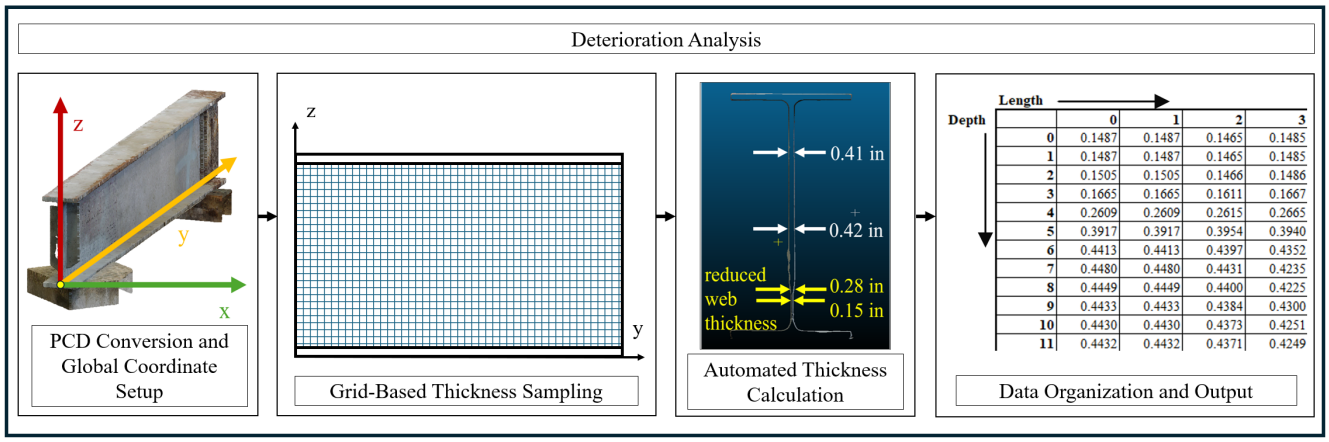

Figure 5.2 Overview of Deterioration Analysis Using Point Cloud Model.

- *PCD Conversion and Global Coordinate Setup*: PCD from scanning devices is typically in text format, listing x, y, and z coordinates (with optional intensity or color channels). The framework converts these raw files to CSV format, defining a global coordinate system for consistent reference across scans. For instance, the lower-left corner of the girder web can be set as the origin (0,0,0), aligning the web along the x and y axes. This standardizes spatial references and simplifies calculations.
- *Grid-Based Thickness Sampling*: After establishing a global coordinate system, the framework subdivides the web into a user-defined grid, typically 1 in. × 1 in. cells. Smaller cells capture more detail but increase computation time and data volume, while larger cells process more quickly but with reduced resolution. Each grid cell represents a local area where the framework computes web thickness.
- *Automated Thickness Calculation*: Within each cell, the framework (using the provided Python scripts) identifies PCD corresponding to the front and back surfaces of the web. The framework calculates web thickness by determining the shortest distance between these opposing surfaces, effectively subtracting

the z-coordinate of the inside surface from the outside surface. Algorithmic checks remove noise points and outliers to ensure accurate thickness measurement.

- *Data Organization and Output*: For each grid cell, a CSV file records the resulting thickness value and its spatial coordinates. This consistent set of data points can be visualized as a thickness map or analyzed for material loss trends. Automated processing is essential for speed and accuracy, eliminating manual thickness measurements in girder scans with thousands of points.

5.1.2 Damage Area Identification

This framework identifies damage areas by comparing measured thickness values against a predefined threshold. For steel girders, a commonly used benchmark is 93% of the nominal web thickness (0.93 t_w). Cells or regions below this threshold are flagged as having significant section loss, preventing false alarms from minor surface irregularities and measurement tolerances.

- *Threshold Definition*: The threshold of 0.93 t_w is flexible and can be adjusted based on engineering judgment, material properties, or inspection standards. Using a defined fraction of nominal thickness accounts for manufacturing variations and slight surface wear, preventing misclassification of minor corrosion or measurement noise as critical deterioration.
- *Flagging Damaged Cells*: Once thickness data are compiled in a CSV file (as described in the web thickness measurement process), each grid cell is evaluated against the threshold. Cells with values below 0.93 t_w are automatically tagged as "damage areas." Generating a map of flagged cells is straightforward since the data is structured (including coordinates and thickness values).
- *Mapping and Clustering*: Group flagged cells based on proximity or shared boundaries to represent contiguous corrosion. This consolidates adjacent cells into larger "damage areas" for quantification, such as total area and average thickness reduction.

Figure 5.3 illustrates an example of identified damage areas in a steel girder web. Each cell's thickness is compared to a threshold. The grid size (1 in. × 1 in.) can be adjusted for resolution and data handling. Shaded regions indicate cells below the threshold, highlighting significant section loss.

The framework defines and maps damage areas, facilitating targeted inspections and maintenance. Identifying locations requiring closer examination enables more effective repair planning, load rating assessments, and resource allocation.

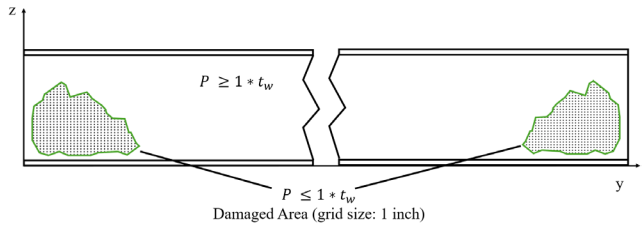

Figure 5.3 An Example of Identified Damage Areas in a Steel Girder Web.

5.2 Residual Strength Estimation Using Empirical Equation

This framework uses empirically derived equations to estimate the residual strength of corroded steel girders. These equations, developed through experimental testing from the previous research (Kanakamedala et al., 2023) and validated against real-world bridge data, use geometric properties of the section loss profile for a rapid assessment.

5.2.1 Key Parameter Determination

The empirical model focuses on four parameters that capture web deterioration. Each parameter is computed from grid-based thickness measurements, particularly in the lower web region near the support where corrosion is most severe. Figure 5.4 depicts the key parameters along with the identified damage areas.

- *Corrosion Length (CL)*: CL is determined by analyzing grid cells in the lower web region near the support. Corroded cells are identified if their thickness is less than 0.93 t_w. These consecutive corroded cells form "corrosion segments" with minor gaps (up to 2 in.) for small discontinuities or noises. The average length of these segments is then calculated, and the final CL is determined by considering the longest possible lengths to ensure conservative results for subsequent analysis.
- *Corrosion Height at Support (CH1) and at Corroded Region End (CH2)*: CH1 is determined from the first three columns near the support (3 in. from the edge) by counting cells below 0.93 t_w . CH2 is evaluated at the corrosion length's tail end (e.g., near CL) with a stricter threshold of 0.98 t_w to differentiate severe deterioration. The maximum value is chosen for conservatism.
- *Effective Remaining Thickness (t_{rem})*: t_{rem} is calculated by averaging the thickness values of the bottom three rows (3 in. from the bottom of the web) up to the bearing length *N*. This region is critical for resisting web local crippling under concentrated loads. For instance, a nominal thickness t_w of 0.50 in. and a measured t_{rem} of 0.30 in. indicates substantial section loss, signaling potential vulnerability near the support (Kanakamedala et al., 2023).
- *Thickness Loss (t_{loss})*: t_{loss} quantifies the absolute extent of corrosion by subtracting t_{rem} from t_w. A higher value suggests more severe degradation and reduced load-carrying capacity.

After determining these parameters, these parameters are converted into dimensionless ratios to ensure broad applicability:

$$\beta = \frac{CL}{h_w} \left(capped\ at\ 1.0\ if\ CL\ exceeds\ the\ web\ height \right)$$

$$\alpha = \frac{t_{loss}}{t_w} \qquad \gamma = \frac{\mathrm{CH1}}{h_w} \qquad \kappa = \frac{\mathrm{CH2}}{h_w}$$

5.2.2 Residual Strength Calculation

Using the above parameters, the framework, first, calculates reduction factors for web local crippling (φ_{rsdl_wlc}) and shear capacity (φ_{rsdl_shear}). These factors are multiplied by nominal strengths (R_n and V_n) established in American Association of State Highway and Transportation Officials (AASHTO; Kanakamedala et al., 2023) or similar specifications. For example, a computed $\varphi_{rsdl\_wlc} = 0.85$ indicates a 15% reduction in local

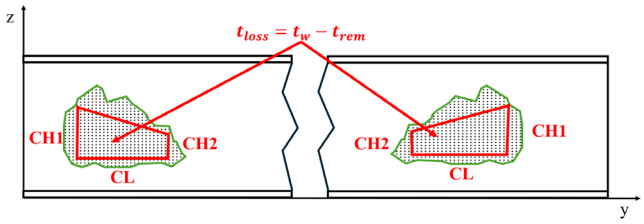

Figure 5.4 An Example of Four Parameters Along With the Identified Damage Areas.

Algorithm Residual Strength Estimation for Corroded Steel Girders

Require: Web thickness (t_w), web height (h_w), corrosion parameters (CL, CH1, CH2, t_{rem})
Ensure: Residual web local crippling strength ($R_{residual}$), Residual shear strength ($V_{residual}$)
Step 1: Calculate dimensionless parameters
$\beta \leftarrow \min(CL/h_w, 1.0)$ {Normalized corrosion length}
$\alpha \leftarrow (t_w - t_{rem})/t_w$ {Normalized thickness loss}
$\gamma \leftarrow CH1/h_w$ {Normalized corrosion height at support}
$\kappa \leftarrow CH2/h_w$ {Normalized corrosion height at end}
Step 2: Calculate nominal strengths
$R_n \leftarrow 0.4t_w^2[1 + (4N/D - 0.2)(t_w/t_f)^{1.5}]\sqrt{EF_y t_f/t_w}$ {Web local crippling}
$V_n \leftarrow 0.6F_y t_w DC_{v1}$ {Shear capacity}
Step 3: Calculate reduction factors
$\phi_{rsdl\_wlc} \leftarrow 0.8 - 1.4e^{-\beta/3}\alpha$ {Web local crippling}
$\phi_{rsdl\_shear} \leftarrow 1 - 0.4\beta(0.7\gamma + 0.5\kappa)\alpha$ {Shear}
Step 4: Calculate residual strengths
$R_{residual} \leftarrow \phi_{rsdl\_wlc} \times R_n$
$V_{residual} \leftarrow \phi_{rsdl\_shear} \times V_n$
return $R_{residual}$, $V_{residual}$

Figure 5.5 Pseudo-code of the algorithms of the Framework that calculates residual strengths.

crippling capacity due to corrosion. Because these equations are empirically derived, they offer computational simplicity while retaining the accuracy needed for most routine inspections.

The framework provides a computer algorithm that can calculate (1) dimensionless parameters ($\alpha, \beta, \gamma, and \kappa$), (2) nominal strengths (R_n and V_n), (3) reduction factors (φ_{rsdl_wlc} and φ_{rsdl_shear})., and (4) residual strengths ($R_{residual}$ and $V_{residual}$). Figure 5.5 shows the pseudo-code of the algorithms of the framework that calculates residual strengths.

5.3 Residual Capacity Evaluation Through FEM Model

This framework uses automated FEA with Python scripting and Abaqus to provide in-depth structural assessments for bridges with complex geometries and critical loading conditions. It constructs detailed FEM models from processed PCD, runs analyses like static capacity checks and buckling studies, and provides high-fidelity insights into potential failure modes. The automated approach minimizes manual intervention, enhances repeatability, and allows rapid evaluations across large bridge inventories or time-sensitive projects, enabling engineers to pinpoint localized weaknesses and accurately estimate load-carrying capacity.

5.3.1 Automated FEM Model Development

The framework implements a sophisticated computational pipeline that transforms PCD into FEM for structural assessment. This process employs parametric scripting to generate, configure, and execute advanced FEA in Abaqus, significantly enhancing efficiency and consistency compared to manual modeling approaches. The workflow begins with systematic processing of PCD through several key stages:

1. *Geometric Model Construction*: The framework first extracts critical girder dimensions from standardized data files, including flange dimensions, web geometry, and overall member length. These parameters drive the parametric construction of the W-section geometry, ensuring accurate representation of the base structural form before deterioration mapping.
2. *Material Property Integration*: Material characteristics are incorporated through a unified property assignment system that includes elastic parameters (modulus of elasticity and Poisson's ratio), mass properties, and nonlinear constitutive relationships. The system supports bilinear and multilinear stress-strain formulations to accurately represent steel behavior in both elastic and plastic regimes.
3. *Systematic Grid Partitioning*: A key innovation is the implementation of an automated partitioning system that creates a high-resolution grid network (typically at 1 in. × 1 in. spacing) across the web surface. This partitioning strategy establishes the foundation for precise mapping of non-uniform thickness distributions caused by corrosion. The system generates orthogonal datum planes that systematically segment the model, creating discrete regions for thickness assignment.
4. *Thickness Mapping from PCD*: The framework implements a data-driven thickness assignment algorithm that reads processed thickness measurements from the point cloud analysis and systematically transfers these values to corresponding regions in the FEM. This process creates a high-fidelity digital twin of the corroded girder, preserving the spatial variation in web thickness caused by deterioration.
5. *Mesh Generation and Assembly*: The system employs automated mesh generation algorithms optimized for shell elements (specifically S4R elements), which are particularly effective for modeling thin-walled structures like steel girders. Mesh refinement parameters are configured to balance computational efficiency with solution accuracy. The meshed components are then assembled with predefined connection sets for boundary conditions and load application regions.
6. *Boundary Condition and Load Configuration*: The framework includes predefined templates for support conditions (pinned and roller supports), lateral bracing configurations, and loading scenarios based on standardized structural assessment requirements. These templates are automatically applied to the relevant geometric entities in the model, ensuring consistent analysis setup.

5.3.2 Residual Strength and Failure Mode Assessment

The framework implements multiple analysis methodologies to comprehensively evaluate the corroded girder's structural behavior:

1. *Multianalysis Configuration*: The system automatically configures both static strength and eigenvalue buckling analyses to assess different potential failure modes. The static analysis employs the modified Riks method to capture postbuckling behavior and geometric nonlinearity, while the eigenvalue analysis identifies critical buckling modes and load factors.
2. *Comprehensive Response Monitoring*: The framework establishes systematic output requests to capture critical structural responses, including section forces, stress distributions, and deformation

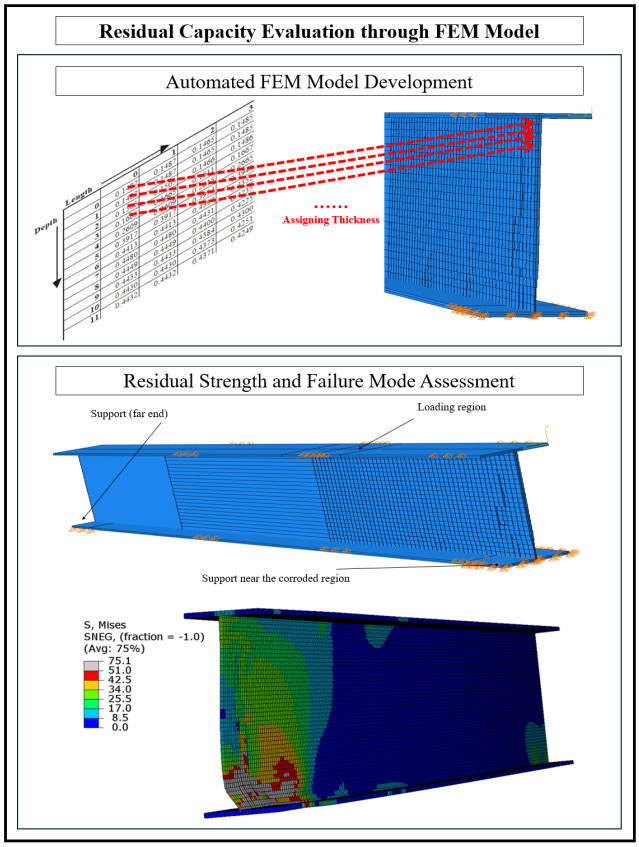

Figure 5.6 Overview of Residual Capacity Evaluation Through FEM Model.

patterns. These outputs are configured for optimal postprocessing and visualization of results.

3. *Initial Imperfection Integration*: A sophisticated feature of the framework is its ability to incorporate realistic geometric imperfections derived from eigenvalue buckling modes. This approach enables more accurate prediction of ultimate capacity by accounting for geometric instability phenomena that are particularly relevant for corroded steel girders.
4. *Analysis Execution Management*: The framework generates complete analysis specifications and manages execution parameters, enabling seamless integration with high-performance computing resources when needed. This approach supports both individual analyses and parametric studies to evaluate sensitivity to various deterioration patterns.

This automated finite element modeling approach significantly accelerates the evaluation process while ensuring methodological consistency and reproducibility. By eliminating labor-intensive model development tasks and providing standardized analysis configurations, the framework enables transportation agencies to efficiently evaluate multiple bridges or monitor deterioration progression over time with high reliability and technical rigor.

5.4 Case Study: Implementation of Proposed Framework

An 18 ft W24×68 steel girder, salvaged from a demolished bridge in Indianapolis, Indiana, was selected to demonstrate the proposed framework. The girder has a nominal web thickness of 0.5 in. and a web height of 24 in. The research team scanned the girder using close-range photogrammetry, and conducted the experiments at Bowen Laboratory. By focusing on a single girder in a controlled environment, the framework's accuracy and reliability could be evaluated alongside actual load-carrying experiments. Figure 5.7 and Figure 5.8 and provide an overview of the girder's point cloud model in both side elevation and cross-sectional views, respectively.

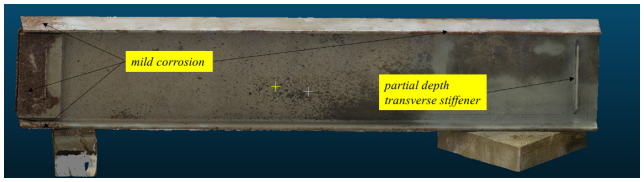

Figure 5.7 Point Cloud Model: Side Elevation View.

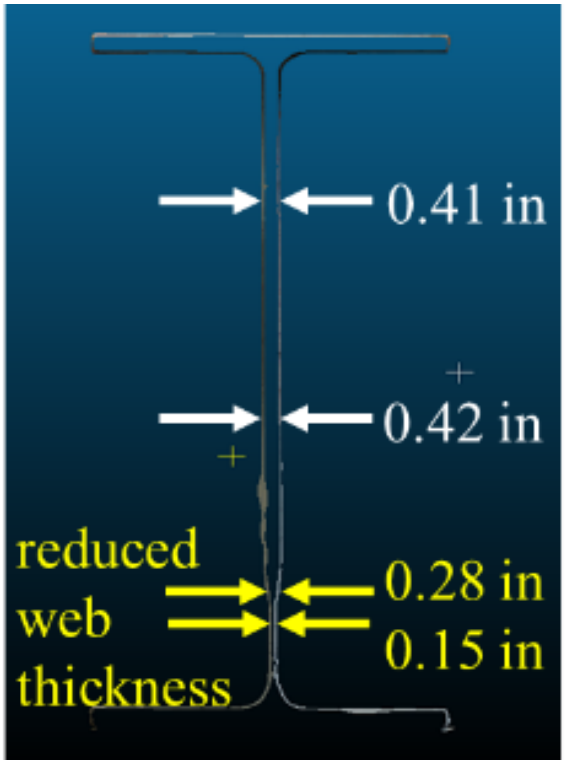

Figure 5.8 Point Cloud Model: Cross Sectional View.

5.4.1 (1) Deterioration Analysis using Point Cloud Model

First, the point cloud model was converted to a CSV file with a global coordinate system to identify the girder's damaged area. A grid spacing of 1 in. × 1 in. was implemented up to a length of 48 in., as illustrated in Figure 5.9. Within this grid, the framework calculates local thickness by comparing points on the web's interior and exterior surfaces. Figure 5.10 depicts a contour plot of the remaining web thickness derived from this

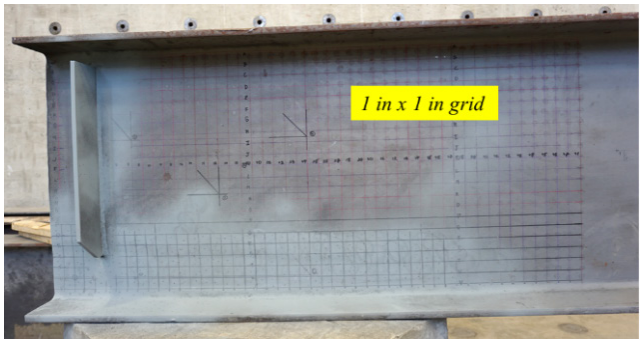

Figure 5.9 Created Grid System to the Scanned Girder.

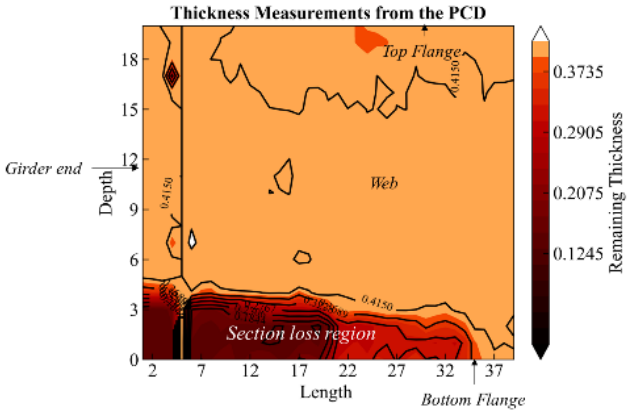

Figure 5.10 Contour plots of web thickness measured from the point cloud.

process; the left side corresponds to the girder end, and the bottom represents the lower flange.

Based on these contour plots, significant section loss appears to follow a trapezoidal pattern, especially near the girder end (0–20 in.). In these regions, the remaining thickness measures about 0.1245 in., indicating notable deterioration. From 20 in. to 30 in., the girder exhibits less severe section loss, with thicknesses around 0.2905 in., illustrated by the light brown shading in the contour plot.

To validate these point cloud–based measurements, the girder's web thickness was also assessed using a T-Mike BTM ultrasonic thickness gauge (UT). Traditional measurement tools (e.g., calipers or tape measures) can provide spot checks but are often insufficient for comprehensive verification across an entire girder. Therefore, UT readings were collected at each 1 in. × 1 in. grid cell up to 48 in., resulting in approximately 1,100 data points. Figure 5.11 shows the resulting contour plot of web thickness based on UT measurements, while Figure 5.12 illustrates the accuracy of the point cloud model by comparing thickness values at each grid cell. The accuracy metric is computed as follows:

$$\text{Accuracy} = 1 - \frac{(\text{thickness from PCD}) - (\text{thickess from UT})}{(\text{thickess from UT})}$$

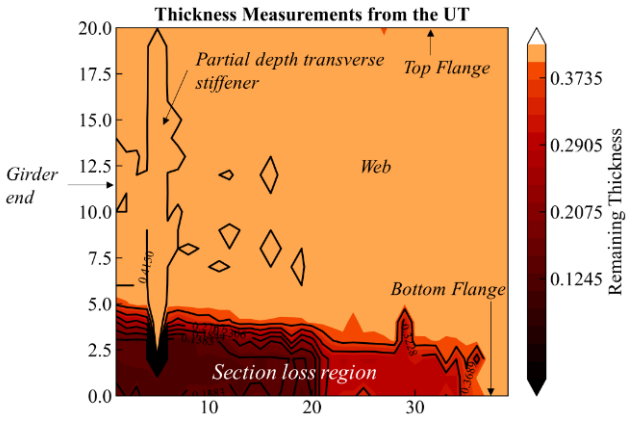

Figure 5.11 Contour Plot of Remaining Web Thickness..

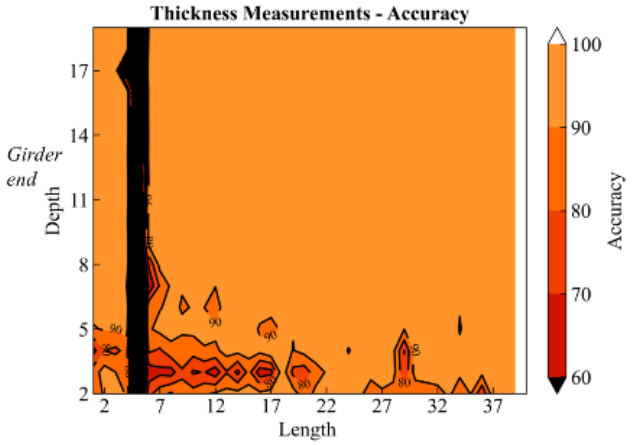

Figure 5.12 Accuracy of Each Point Cloud Model.

Analysis of these contour plots reveals that the point cloud model achieves approximately 90% accuracy in most areas of the web. In a few localized regions, accuracy ranges from 70% to 80%, potentially influenced by scanning angles, surface reflectivity, or minor registration errors.

Overall, this validation demonstrates the framework's capacity to generate high-resolution thickness data across an entire girder web, offering comprehensive insights into section loss patterns. The consistency between point cloud–based measurements and UT assessments confirms that automated scanning and data processing can accurately capture web deterioration and facilitate early intervention strategies.

5.4.2 (2) Residual Strength Estimation using Empirical Equation

The process involves extracting key geometric parameters from a deterioration analysis and using them to calculate strength reduction factors for web local crippling and shear capacity. For this case study's W24×68 girder, the following corrosion parameters were extracted:

- Corrosion Length (CL): 37 in.
- Effective Remaining Thickness: 0.313 in.

- Corrosion Height near Support (CH1): 6 in.
- Corrosion Height at Corrosion End (CH2): 1 in.

Based on this identified damaged area, four dimensionless ratios and the girder's thickness loss have been calculated as follows:

- The thickness loss (t_{loss}) due to corrosion:

$$t_{loss} = t_w - t_{rem} = 0.5 - 0.313 = 0.187\,\text{in.}$$

- β: Ratio of corrosion length to web height, capped at 1.0

$$\beta = \min\left(\frac{CL}{h_w}, 1.0\right) = \min\left(\frac{37}{24}, 1.0\right) = \min(1.542, 1.0) = 1.0$$

- α: Ratio of thickness loss to nominal thickness

$$\alpha = \frac{t_{loss}}{t_w} = \frac{0.187}{0.5} = 0.374$$

- γ: Ratio of corrosion height near the support to web height

$$\gamma = \frac{CH1}{h_w} = \frac{6}{24} = 0.25$$

- κ: Ratio of corrosion height at the corrosion end to web height

$$\kappa = \frac{CH2}{h_w} = \frac{1}{24} \approx 0.042$$

Based on these four dimensionless ratios and the calculated thickness loss, we compute the reduction factors for web local crippling (ϕ_{rsdl_wlc}) and shear capacity (ϕ_{rsdl_shear}):

- Web Local Crippling Reduction Factor

$$\phi_{rsdl\_wlc} = 0.8 - \left(1.4 \times e^{-\frac{1}{3}\beta} \times \alpha\right)$$

$$\phi_{rsdl\_wlc} = 0.8 - \left(1.4 \times e^{-\frac{1}{3}\times 1.0} \times 0.374\right)$$

$$\phi_{rsdl\_wlc} = 0.8 - 0.375 \approx 0.425$$

- Shear Capacity Reduction Factor

$$\phi_{rsdl\_shear} = 1 - 0.4 \times \beta \times (0.7\gamma + 0.5\kappa) \times \alpha$$

$$\phi_{rsdl\_shear} = 1 - 0.4 \times 1.0 \times (0.7 \times 0.25 + 0.5 \times 0.042) \times 0.374$$

$$\phi_{rsdl\_shear} = 1 - 0.0293 \approx 0.971$$

The team used the nominal strengths for the W24x68 girder, provided in AASHTO's (2020) *LRFD Bridge Design Guide*. The residual strengths are calculated as follows:

- Nominal Web Local Crippling Strength:

$$R_n = 169.35 \text{ kips}$$

- Nominal Shear Strength:

$$V_n = 307.18 \text{ kips}$$

- Residual Web Local Crippling Strength (Bearing Capacity):

$$R_{residual} = R_n \times \phi_{rsdl\_wlc} = 169.35 \times 0.425 \approx 71.97 \text{ kips}$$

- Residual Shear Strength:

$$V_{Residual} = V_n \times \phi_{rsdl\_shear} = 307.18 \times 0.971 \approx 298.22 \text{ kips}$$

The calculated residual web local crippling strength of 76.54 kips shows a significant reduction from the nominal value of 169.35 kips, indicating a substantial loss of capacity due to corrosion. Interestingly, some results provided elsewhere suggest a residual crippling strength of 52.41 kips, which is even lower. This discrepancy could stem from adjustments in the empirical method or different input values, and it underscores the importance of validating these estimates with a more detailed FEA, especially when significant strength reductions are observed. The residual shear strength of 298.22 kips remains close to the nominal value of 307.18 kips, suggesting that shear capacity is less affected by the corrosion in this case.

5.4.3 (3) Residual Capacity Evaluation through FEM Model

To complement the empirical estimates of residual strength developed earlier—particularly for girders with significant deterioration, a detailed FEA was conducted using Abaqus. In order to compare the results of FEM model, a large-scale experimental investigation was also performed to establish a reliable benchmark for the FEA. Residual web local crippling strength and shear strength were estimated based on the deterioration patterns observed in point cloud analysis (Figure 5.7, Figure 5.8, Figure 5.13, and Figure 5.14). The resulting section loss profile, shown in a contour plot (Figure 5.10), matched Figure 5.11 and Figure 5.12, ensuring a valid basis for comparing residual capacity between experimental and numerical approaches.

The experimental setup involved applying a load with an actuator positioned 40 in. from the girder's end (Figure 5.15), simulating real-world loading conditions. Vertical displacement

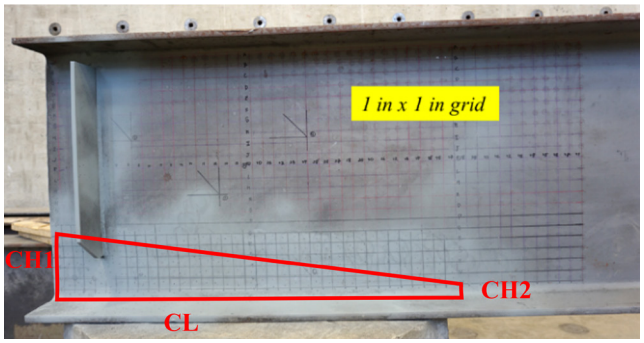

Figure 5.13 Created Grid System to the Scanned Girder.

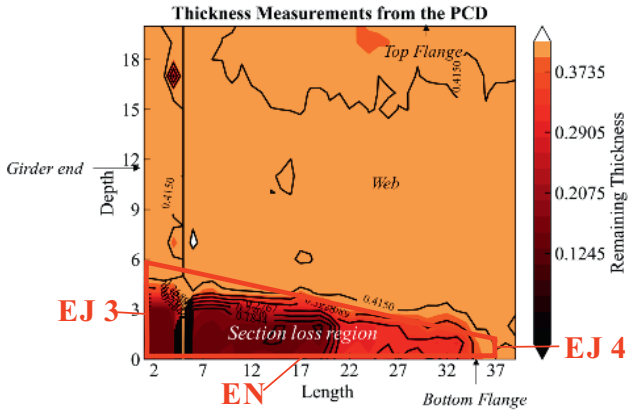

Figure 5.14 Contour Plots of Web Thickness Measured From the Point Cloud.

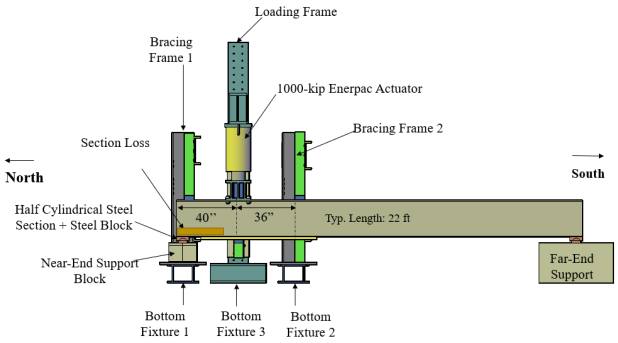

Figure 5.15 Schematic View of the Test Set Up.

of the bottom flange was measured in the loading region. The girder was supported in a simply supported configuration using two steel blocks, allowing for rotations, while lateral stability was ensured through bracing frames. The section loss contour plot is shown in Figure 5.16. This contour plot is created as subtracting remaining web thickness (Figure 5.11) from the original web thickness.

The FEA model was developed in Abaqus using S4R shell elements, 4-node doubly curved elements suitable for thick or thin shells, with reduced integration and hourglass control for computational efficiency. A key feature was the accurate assignment of web thickness, extracted from point cloud models via automated Python scripting. This mirrored the thickness data used in the empirical estimates (e.g., an effective remaining thickness of 0.313 in. near the support). The top and bottom flanges were assigned a nominal thickness of 0.585 in., and a uniform mesh size of 0.5 in. was applied throughout the model (Figure 5.17).

Boundary conditions replicated the experimental setup: the deteriorated end was modeled as a pinned support with translational restraints, while the opposite end was constrained vertically as a roller support. Lateral restraints were applied to the top and bottom flanges at the section loss region and 36 in. from the loading point to prevent lateral buckling. Displacement-controlled loading was applied 40 in. from the girder's end,

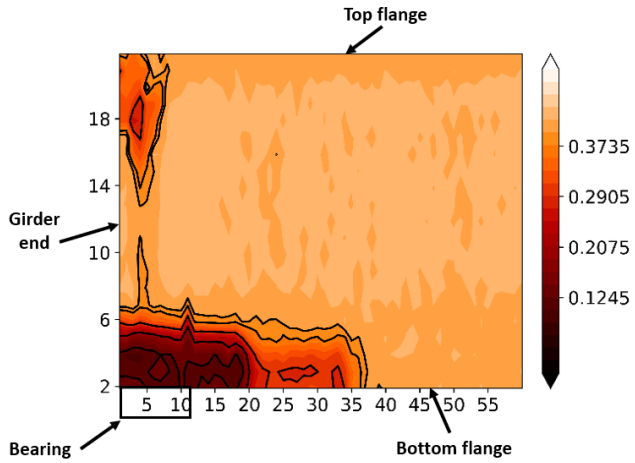

Figure 5.16 Experimental Specimen - Section Loss Contour Plot.

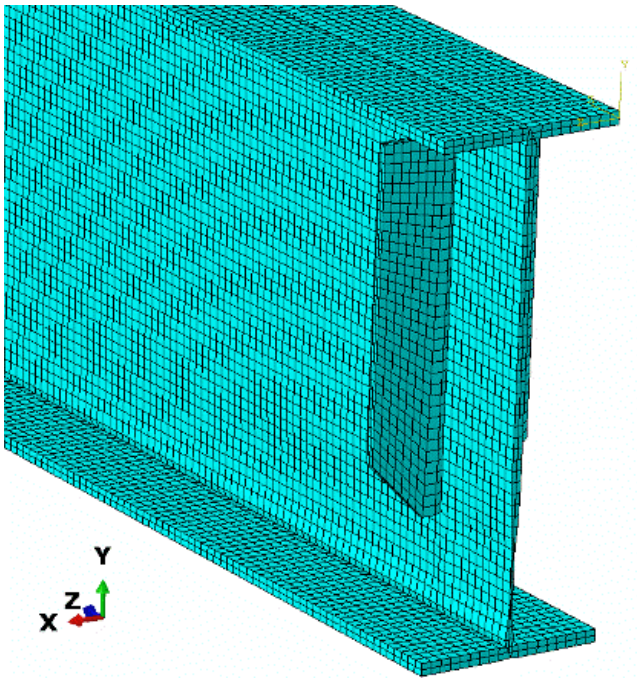

Figure 5.17 Numerical Model Girder Modelled With Shell Element With Thickness Measurements From the Point Cloud Model.

consistent with the experiment. Due to anticipated instability from section loss, the static RIKS method was used to capture nonlinear behaviors like web local crippling. Material properties adhered to ASTM E8 standards (Figure 5.18).

Both the experiment and FEA identified web local crippling as the dominant failure mode (Figure 5.20). The experimental maximum applied force was 48.5 kips, while the FEA predicted a residual capacity of 50.01 kips—a difference of approximately 3.1%. This close agreement validates the FEA model's accuracy in capturing initial stiffness and postpeak behavior, as shown in Figure 5.20, which compares the applied force-to-displacement responses.

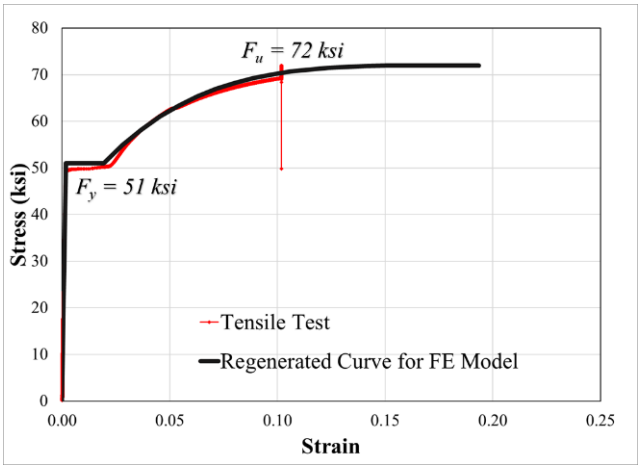

Figure 5.18 Numerical Model Material Property.

These results also tie back to the empirical estimates from earlier sections. For Bridge A, the empirical method estimated a residual web local crippling strength of 76.54 kips, while the FEA provided a refined prediction of 50.01 kips (Figure 5.20). This discrepancy highlights the conservative nature of empirical approaches and underscores the value of FEA for critical cases requiring precise capacity assessments to inform maintenance decisions.

5.5 Summary of the Proposed Framework

The proposed framework uses 3D scanning, empirical strength equations, and automated finite element modeling to evaluate corroded steel girders. It creates detailed visual representations of corrosion severity, calculates capacity reduction factors, and provides high-fidelity insights into stress distributions and failure modes.

Key contributions include converting point cloud scans into grid-based CSV files to measure local thickness and identify damage areas. The framework balances accuracy and computational efficiency, enabling engineers to handle large-scale scans with sufficient detail. Empirical equations focus on corrosion-related parameters to swiftly estimate girder load-carrying capacity. These methods are accurate for routine inspections and allow agencies to prioritize repairs. In severe deterioration cases or with intricate girder geometries, an automated FEA process within Abaqus refines capacity predictions. Python scripting streamlines geometry creation, mesh generation, boundary condition assignment, and result extraction processes.

A controlled test environment with an 18 ft W24×68 steel girder validated the framework's effectiveness. Point cloud measurements, ultrasonic thickness readings, empirical estimates, and experimental load tests were conducted. 3D scanning outputs showed approximately 90% agreement with ultrasonic measurements, confirming the reliability of deterioration analysis. The FEA approach accurately predicted capacity within 3.1% of experimental results, underscoring the model's accuracy in assessing corroded girder sections.

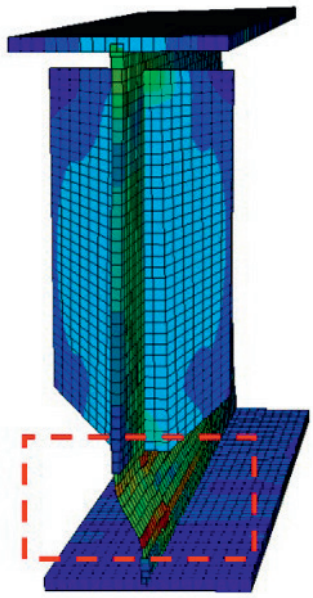

(a)

(b)

Figure 5.19 Failure Mode – Web Local Crippling Failure.

This framework integrates scanning, empirical calculations, and advanced modeling to address the varied needs of infrastructure agencies:

- *Speed and cost-effectiveness*: Rapid evaluation via point cloud scanning and empirical strength predictions reduces inspection times and costs.
- *Adaptability*: Parameter-based thresholds and grid sizes accommodate varying accuracy, geometries, and corrosion severity.
- *Scalability*: Automated finite element processes assess large inventories without manual effort, supporting proactive maintenance.

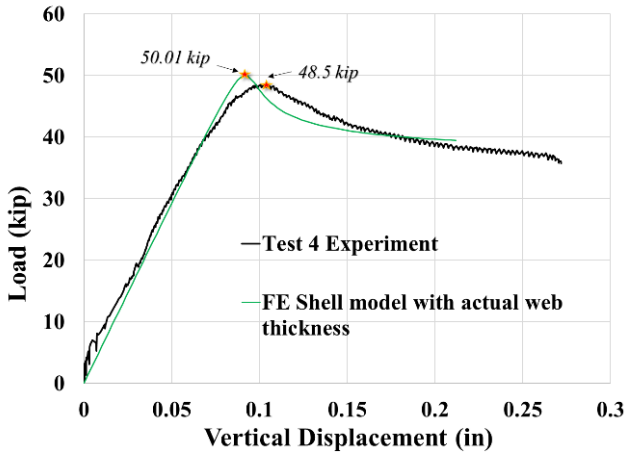

Figure 5.20 Comparison of FEM With Experimental Results (Web Clipping Capacity).

- *Risk mitigation*: In-depth failure mode insights from FEM analysis allow confident decisions about load restrictions, repairs, or retrofits.

The multitiered approach ensures bridge owners and engineers tailor analysis to each structure's condition and importance, maximizing efficiency and safety.

6. CONCLUSION

6.1 Summary

This study explored the feasibility of 3D scanning technologies for bridge inspection and structural assessment, focusing on steel girder condition evaluation and residual strength estimation. The research compared TLS, CRP, and UAV-based photogrammetry, determining their effectiveness in capturing corrosion, section loss, and deformation in steel bridge girders. A comprehensive scanning framework was developed, integrating data acquisition, deterioration analysis, and strength estimation to support transportation agencies in improving bridge inspection efficiency.

Key findings demonstrated that UAV-based photogrammetry provides a cost-effective and operationally efficient solution for capturing complex bridge geometries, making it preferable for large-scale inspections. TLS excelled in global dimensional accuracy, while CRP proved more reliable in web thickness measurements. Combining these technologies in a hybrid approach maximizes coverage and accuracy. The study also highlighted environmental and operational challenges, such as lighting conditions, wind effects, and access constraints, that impact scanning effectiveness in real-world bridge settings.

6.2 Implementation of the Proposed Framework for Bridge Assessment

The proposed 3D scanning framework provides a systematic approach to assessing corroded steel girders and estimating their residual capacity. The framework consists of three key components:

- Deterioration Analysis using PCD: Enables precise mapping of section loss, identifying critical damage areas.
- Residual Strength Estimation using Empirical Equations: Offers rapid capacity assessments based on predefined models.
- Residual Capacity Evaluation through FEM Modeling: Provides high-fidelity stress analysis, recommended when empirical estimates are insufficient.

A case study validated the framework, demonstrating that point cloud-derived thickness measurements align closely with ultrasonic thickness data (90% agreement). Empirical strength estimates provided a quick and reliable assessment of girder performance, while FEA offered detailed insights into failure modes and structural behavior. The results confirm that this multitiered assessment strategy improves decision-making for bridge maintenance and rehabilitation planning.

6.3 Implementation of the Proposed Guideline for 3D Scanning

Based on laboratory and field testing, a practical guideline was developed for systematic bridge scanning. The guideline covers:

- Technology selection: Recommends UAV photogrammetry for large-scale inspections, with TLS and CRP used for targeted high-precision measurements.
- Field preparation and operations: Defines optimal scanning parameters, flight paths, and environmental considerations to enhance data quality.
- Postprocessing and data management: Establishes workflows for point cloud processing, quality control, and integration with structural assessment tools.

Field implementations demonstrated that adapting scanning protocols to real-world conditions—including variable lighting, wind exposure, and confined spaces—is essential for achieving high-quality data. The research also identified best practices for image exposure settings, multiplatform scanning integration, and feature detection, ensuring consistent, accurate, and repeatable scanning results.

REFERENCES

Ameli, Z., Aremanda, Y., Friess, W. A., & Landis, E. N. (2022). Impact of UAV hardware options on bridge inspection mission capabilities. *Drones*, *6*(3), 64. https://doi.org/10.3390/drones6030064

American Association of State Highway and Transportation Officials. (2020). *LRFD bridge design specifications* (9th edition). American Association of State Highway and Transportation Officials.

Barth, K. E., & Wu, H. (2006). Efficient nonlinear finite element modeling of slab on steel stringer bridges. *Finite Elements in Analysis and Design*, *42*(14–15), 1304–1313. https://doi.org/10.1016/J.FINEL.2006.06.004

Beainy, F., Commuri, S., & Zaman, M. (2011). Quality assurance of hot mix asphalt pavements using the intelligent asphalt compaction analyzer. *Journal of Construction Engineering and Management*, *138*(2), 178–187. https://doi.org/10.1061/(asce)co.1943-7862.0000420

Bolourian, N., & Hammad, A. (2020). LiDAR-equipped UAV path planning considering potential locations of defects for bridge inspection. *Automation in Construction*, *117*, 103250. https://doi.org/10.1016/J.AUTCON.2020.103250

Chen, S., Laefer, D. F., Mangina, E., Iman Zolanvari, S. M., & Byrne, J. (2019). UAV bridge inspection through evaluated 3D reconstructions. *Journal of Bridge Engineering*, *24*(4), 05019001. https://doi.org/10.1061/(ASCE)BE.1943-5592.0001343

Elkawas, A. A., Hassanein, M. F., & El-Boghdadi, M. H. (2017). Numerical investigation on the nonlinear shear behaviour of high-strength steel tapered corrugated web bridge girders. *Engineering Structures*, *134*, 358–375. https://doi.org/10.1016/J.ENGSTRUCT.2016.12.044

Gyetvai, N., Truong-Hong, L., & Laefer, D. F. (2018). Laser scan-based structural assessment of wrought iron bridges: Guinness Bridge, Ireland. *Proceedings of the Institution of Civil Engineers—Engineering History and Heritage*, *171*(2), 76–89. https://doi.org/10.1680/JENHH.17.00018

Horan, R. D., Chang, G. K., Xu, Q., & Gallivan, V. L. (2012). Improving quality control of hot-mix asphalt paving with intelligent compaction technology. *Transportation Research Record*, *2268*(1), 82–91. https://doi.org/10.3141/2268-10

Indiana Department of Transportation. (2022). *Indiana Department of Transportation standard specifications*. https://www.in.gov/dot/div/contracts/standards/book/sep21/2022%20Standard%20Specifications.pdf

Jáuregui, D. V., Tian, Y., & Jiang, R. (2006). Photogrammetry applications in routine bridge inspection and historic bridge documentation. *Transportation Research Record*, *1958*(1), 24–32. https://doi.org/10.1177/0361198106195800103

Jiang, R., & Jáuregui, D. v. (2010). Development of a digital close-range photogrammetric bridge deflection measurement system. *Measurement*, *43*(10), 1431–1438. https://doi.org/10.1016/J.MEASUREMENT.2010.08.015

Jin, D., Ge, D., Chen, S., Che, T., Liu, H., Malburg, L., & You, Z. (2021). Cold in-place recycling asphalt mixtures: Laboratory performance and preliminary M-E design analysis. *Materials*, *14*(8), 2036. https://doi.org/10.3390/ma14082036

Kanakamedala, D., Seo, J., Varma, A. H., Connor, R. J., & Tarasova, A. (2023). *Shear and bearing capacity of corroded steel beam bridges and the effects on load rating* (Joint Transportation Research Program Report No. FHWA/IN/JTRP-2023/11). Purdue University. https://doi.org/10.5703/1288284317634

Khaloo, A., Lattanzi, D., Cunningham, K., Dell'Andrea, R., & Riley, M. (2018). Unmanned aerial vehicle inspection of the Placer River Trail Bridge through image-based 3D modelling. *Structure and Infrastructure Engineering*, *14*(1), 124–136. https://doi.org/10.1080/15732479.2017.1330891

Lu, R., & Brilakis, I. (2017). Recursive segmentation for as-is bridge information modelling. In *Lean and Computing in Construction Congress (LC3): Volume I* (pp. 209–217). Joint Conference on Computing in Construction (JC3), Heraklion, Greece. https://doi.org/10.24928/JC3-2017/0020

Metni, N., & Hamel, T. (2007). A UAV for bridge inspection: Visual servoing control law with orientation limits. *Automation in Construction*, *17*(1), 3–10. https://doi.org/10.1016/J.AUTCON.2006.12.010

Miller, S. R., Hartmann, T., & Dorée, A. G. (2011). Measuring and visualizing hot mix asphalt concrete paving operations. *Automation in Construction*, *20*(4), 474–481. https://doi.org/10.1016/j.autcon.2010.11.015

Mohammadi, M., Rashidi, M., Mousavi, V., Karami, A., Yu, Y., & Samali, B. (2021). Case study on accuracy comparison of digital twins developed for a heritage bridge via UAV photogrammetry and terrestrial laser scanning. In *Proceedings of the 10th international conference on Structural Health Monitoring of Intelligent Infrastructure (SHMII)* (pp. 1713–1720). https://researchdirect.westernsydney.edu.au/islandora/object/uws%3A62196

Omar, T., & Nehdi, M. L. (2017). Remote sensing of concrete bridge decks using unmanned aerial vehicle infrared thermography. *Automation in Construction*, *83*, 360–371. https://doi.org/10.1016/j.autcon.2017.06.024

Pinto, L., Bianchini, F., Nova, V., & Passoni, D. (2020). Low-cost UAS photogrammetry for road infrastructures' inspection. *The International Archives of the Photogrammetry, Remote Sensing and Spatial Information Sciences*, *XLIII-B2-2020*, 1145–1150. https://doi.org/10.5194/ISPRS-ARCHIVES-XLIII-B2-2020-1145-2020

Popescu, C., Täljsten, B., Blanksvärd, T., & Elfgren, L. (2019). 3D reconstruction of existing concrete bridges using optical methods. *Structure and Infrastructure Engineering*, *15*(7), 912–924. https://doi.org/10.1080/15732479.2019.1594315

Tzortzinis, G., Ai, C., Breña, S. F., & Gerasimidis, S. (2022). Using 3D laser scanning for estimating the capacity of corroded steel bridge girders: Experiments, computations and analytical solutions. *Engineering Structures*, *265*, 114407. https://doi.org/10.1016/j.engstruct.2022.114407

Wang, F., Zou, Y., del Rey Castillo, E., Ding, Y., Xu, Z., Zhao, H., & Lim, J. B. P. (2024). Automated UAV path-planning for high-quality photogrammetric 3D bridge reconstruction. *Structure and Infrastructure Engineering*, *20*(10), 1595–1614. https://doi.org/10.1080/15732479.2022.2152840

Yao, Y., & Song, E. (2023). Intelligent compaction methods and quality control. *Smart Construction and Sustainable Cities*, *1*, 2. https://doi.org/10.1007/s44268-023-00004-4

Yiqiu, T., Haipeng, W., Shaojun, M., & Huining, X. (2014). Quality control of asphalt pavement compaction using fibre Bragg grating sensing technology. *Construction and Building Materials*, *54*, 53–59. https://doi.org/10.1016/j.conbuildmat.2013.12.032

APPENDICES

Appendix A. Field Scanning Details

APPENDIX A. Field Scanning Details

1. FAA Drone flight waiver form

The document included as Appendix [X] is a Certificate of Waiver or Authorization (COA) issued by the Federal Aviation Administration (FAA) under 14 CFR 107.41, which represents a critical regulatory requirement for Unmanned Aircraft System (UAS) operations in controlled airspace. This authorization is essential for our research project involving 3D scanning of bridge structures near Purdue University Airport's Class D airspace.

Purpose and Significance

The COA permits specific drone operations within restricted airspace that would otherwise be prohibited under standard Part 107 regulations. For bridge inspection activities utilizing photogrammetric techniques, such authorization is mandatory when operating within the vicinity of airports, as these locations typically fall under controlled airspace designations. The authorization establishes clear operational parameters, including maximum altitude restrictions (150 feet AGL in this case), precise geographical boundaries (designated by coordinates and radius), and temporal limitations.

Project Necessity

Our bridge inspection methodology relies extensively on drone-based photogrammetry for data acquisition, requiring access to specific bridge structures that fall within controlled airspace. Without this authorization, data collection at these crucial sites would be legally impossible, significantly limiting our research scope and practical implementation potential. The authorization enables our team to systematically document bridge conditions while maintaining compliance with federal aviation regulations, ensuring both research integrity and operational safety.

Application Process

Obtaining this authorization required a structured application process through the FAA DroneZone portal (https://faadronezone.faa.gov), which included:

1. Detailed documentation of the proposed operation, including precise coordinates and operational parameters
2. Submission of the remote pilot's certification information and operational qualifications
3. Specification of equipment capabilities and technical specifications
4. Justification of the operation's necessity and purpose

The authorization process typically requires 60–90 days for processing, though expedited authorizations may be available through the Low Altitude Authorization and Notification Capability (LAANC) system for certain airspace classes.

This authorization represents a critical component of our research methodology, enabling the comprehensive 3D scanning approach detailed in the framework section of this report.

DEPARTMENT OF TRANSPORTATION
FEDERAL AVIATION ADMINISTRATION

CERTIFICATE OF WAIVER OR AUTHORIZATION

ISSUED TO: Jiashu Hu
POC PHONE NUMBER: (765) 694-5337

ATTN: Jiashu Hu

This certificate is issued for the operations specifically described hereinafter. No person shall conduct any operation pursuant to the authority of this certificate except in accordance with the standard and special provisions contained in this certificate, and such other requirements of the Federal Aviation Regulations not specifically waived by this certificate.

OPERATIONS AUTHORIZED

Operations under this certificate of authorization are limited to the maximum altitude listed below. This altitude is an absolute value and it shall not be added to the height of any structures.
Class of Airspace: D
At or Below: 150 feet Above Ground Level (AGL)
Location: 40° 24' 32" N, 86° 57' 00" W – Within YELLOW shaded circle – See Attachment 1
Radius: 0.10 NM
Under the Jurisdiction of: Purdue University Airport Traffic Control Tower (LAF ATCT)
Airport Identifier: KLAF

LIST OF WAIVED REGULATIONS BY SECTION AND TITLE

N/A

STANDARD PROVISIONS

1. A copy of the application made for this certificate shall be attached and become a part hereof.
2. This certificate shall be presented for inspection upon the request of any authorized representative of the Federal Aviation Administration, or of any State or municipal official charged with the duty of enforcing local laws or regulations.
3. The holder of this certificate shall be responsible for the strict observance of the terms and provisions contained herein.
4. This certificate is nontransferable.

NOTE - This certificate constitutes a waiver of those Federal rules or regulations specifically referred to above. It does not constitute a waiver of any State law or local ordinance.

SPECIAL PROVISIONS

Special Provisions 1 to 3, inclusive, are set forth in this authorization.

This certificate, 2024-P107-CSA-30044, is effective from September 11, 2024 to October 11, 2024, and is subject to cancellation at any time upon notice by the Administrator or his/her authorized representative.

BY DIRECTION OF THE ADMINISTRATOR

CAROL S LONG
Digitally signed by CAROL S LONG
Date: 2024.09.10 13:02:48 -05'00'

FAA, Central Service Area
(Region)

Dallas W. Lantz
(Signature)

Tactical Operations Team Manager (A), AJV-C23
(Title)

FAA Form 7711-1 (7-74)

SPECIAL PROVISIONS

1. **CONTACT INFORMATION:**

   a. Jiashu Hu is the person designated as responsible for the overall safety of UAS operations under this Certificate of Waiver or Authorization. During UAS operations for on-site communication/recall, the Responsible Person shall be continuously available for direct contact at (765) 694-5337 by LAF ATCT or designated representative.

   b. The Responsible Person listed on this Authorization must maintain a current list of pilots by name and the remote pilot certificate number(s) associated with the Authorization holder's operation. This list must be presented for inspection upon request from the Administrator or an authorized representative.

2. **SCHEDULE OF FLIGHT OPERATIONS:**

   a. This authorization and the Special Provisions shall be in effect between civil sunrise and civil sunset local time, except when complying with the operating requirements in 14 CFR 107.29(a) while operating at night.

   b. UAS flight operations under this certificate are not authorized when LAF ATCT is closed.

   c. This airspace authorization does not relieve the remote pilots from the responsibility to check the airspace they are operating in and comply with all restrictions that may be present in accordance with see 14 CFR 107.45 and 107.49 (a)(2), such as restricted and Prohibited Airspace, Temporary Flight Restrictions, etc.

   d. The operator must contact LAF ATCT at (765)743-2611 at least fifteen (15) minutes prior to operations and immediately upon completion. LAF ATCT may disapprove, terminate, restrict, or delay UAS flight operations covered by this authorization at any time.

3. **EMERGENCY/CONTINGENCY PROCEDURES** - Lost Link/Lost Communications Procedures:

   a. If the UAS loses communications or loses its GPS signal, the UA must return to a pre-determined location within the operating area and land.

   b. The operator must abort the flight in the event of unpredicted obstacles or emergencies.

Attachment 1

OPERATIONS AREA

Class of Airspace: D
At or Below: 150 feet AGL
Location: 40° 24' 32" N, 86° 57' 00" W – Within YELLOW shaded circle
Radius: 0.10 NM

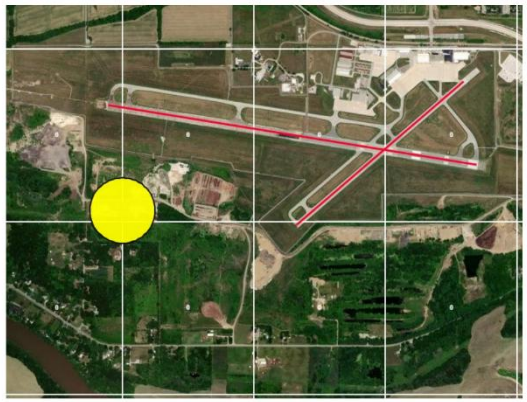

Figure A.1 FAA Certificate of Waiver or Authorization (COA) for UAS Operations in Class D Airspace Near Purdue University Airport (KLAF), September–October 2024.

Table A.1 Data Organization Table.

Date	Folder Name	Objects to Scan	Device Used	Objectives	Folders for Raw Data	Final Products for View
04/20/2023	1-04_20_2023_Bowen_Initial_Scanning	W-section outside of Bowen Lab	Faro LiDAR scanner, Handheld cameras	Test photogrammetry accuracy compared with LiDAR based on literature recommendations	\LiDAR Scanning\W-Section \Raw \Photogrammetry Scanning	\LiDAR Scanning\Trimble Projects\Registered.laz \Photogrammetry Scanning\w-section_photogrametry project\Productions\Production_2 (2)
06/08/2023	2-06_08_2023_Real_Bridge	Real bridge structure	DJI Matrice 300 RTK with P1, Trimble LiDAR-X7	Compare different scanning technologies (drone vs. LiDAR) for future equipment purchasing	\Raw Images Drone \Lidar	Point cloud.las \model\Productions\Production_2
06/16/2023	3-06_16_2023_BowenLab_Lidar	Base section in Bowen Lab	Trimble LiDAR-X7	Create baseline model for comparison with photogrammetry	\	
07/20/2023	4-07_20_2023_BowenLab_Drone_Testing	Double section in Bowen Lab	DJI Matrice 300 RTK with P1	Optimize scanning methodology using different flight paths	*_raw_images	Point CLoud.las *_project/Productions\Production_*/model
08/10/2023	5-08_10_2023_BowenLab_Testing	Double section one in Bowen Lab	DJI Matrice 300 RTK with P1	First formal scanning of double section one	\raw_images	\photogrammetry_project\Productions\Production_2
08/17/2023	6-08_17_2023_BowenLab_Testing	Another double section in Bowen Lab	DJI Matrice 300 RTK with P1	Second formal scanning of another double section	\raw_images	\Photogrammetry Project\Productions\Production_1\Scene

Date	Folder Name	Objects to Scan	Device Used	Objectives	Folders for Raw Data	Final Products for View
09/20/2023	7-09_20_2023_Railway_Bridge	Railway bridge	DJI Matrice 300 RTK with P1	Test path planning for entire bridge level scanning	\Raw_data	
11/13/2023	8-11_13_2023_S_Brite_Reconstruction	Bridge structure in Bowen lab	DJI Matrice 300 RTK with P1	Test modeling results in controlled environment resembling real bridge conditions	\Photogrammetry Data	\Productions\Production_1 (2)
03/19/2024	9-03_19_2024_Exposure_Control_Testing	S-BRITE	Nikon D850, Sony A7M4	Testing manual vs. automatic exposure control for better results	\Group_2\Group_2_data	\Group_2_NIKON_Jiashu_Auto_Exposure\point_cloud_auto exposure.las
04/17/2024	10-04_17_2024_Drone_N9thStRd	N 9th Street Road	DJI Matrice 300 RTK with P1	Test approaching highest model quality by precisely controlling	\DJI_202404251603_001, DJI_202404251603_002, DJI_202404251603_003	\new project\ Productions\ Production(3)
06/17/2024	12-06_17_2024_Sbrite	S-BRITE	DJI Matrice 300 RTK with P1	Test modeling	\Image	\CC_Processing\2024_06_17_Sbrite\Productions
08/27/2024	13-08_27_2024_Sbrite	S-BRITE	Nikon D850, Sony A7M4	Test capturing whole bridge with 2 handheld cameras	\Image	\result
09/09/2024	14-09_09_2024_Drone_N9thStRd	N 9th Street Road	DJI Avata 2	Test feasibility of 3D modeling using Avata 2	\videos	\result

Date	Folder Name	Objects to Scan	Device Used	Objectives	Folders for Raw Data	Final Products for View
09/17/2024	15-09_17_2024_Sbrite	S-BRITE	DJI Avata 2, DJI Matrice 300 RTK with P1/L1	Test reconstructing large area with multiple structures	2024.09.17_sbrite_Bridge\data, 2024.09.17_sbrite_lidar,	

Data Thumbnail

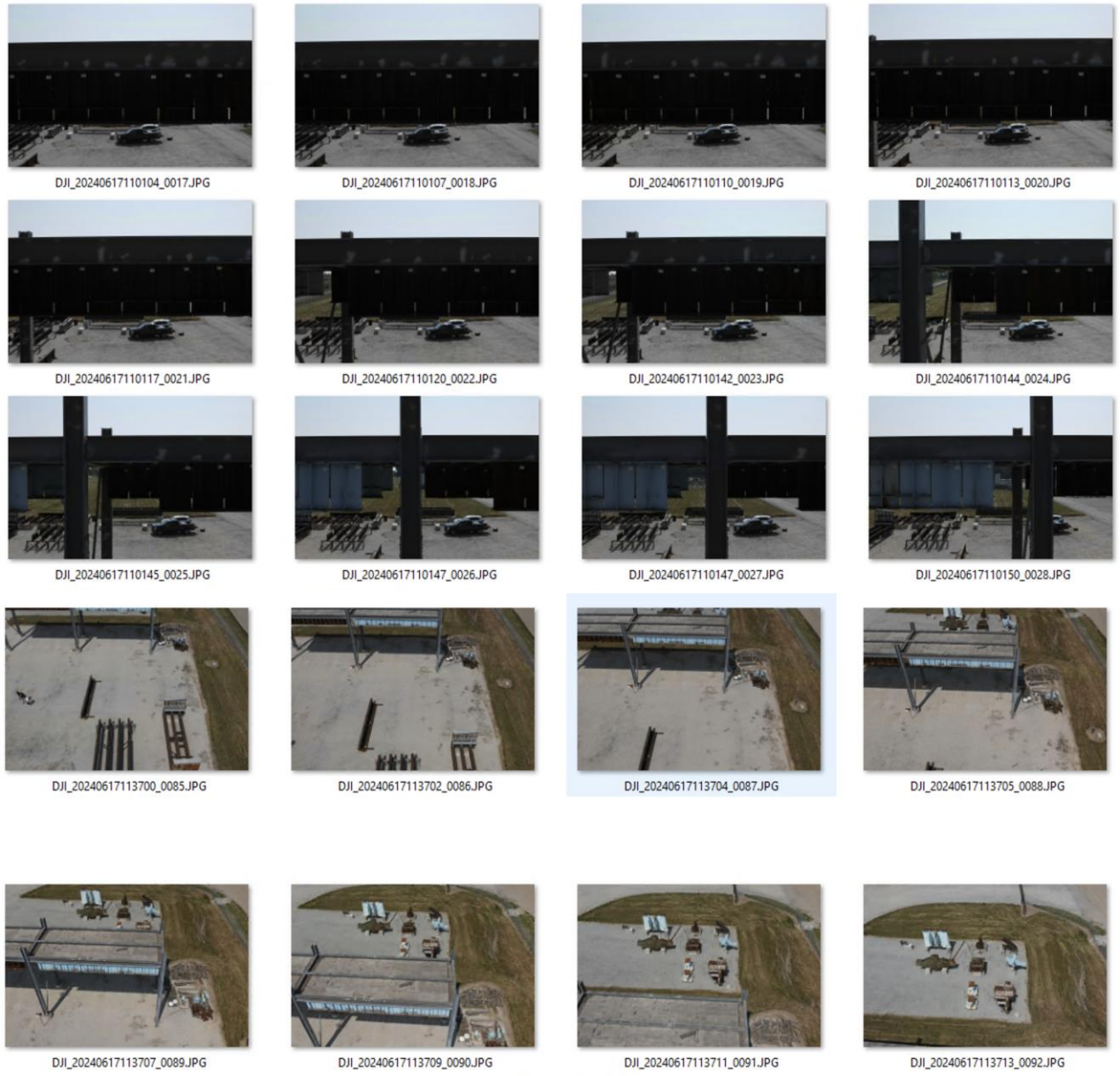

Figure A.2 *Thumbnail Grid of Aerial Photographs Collected by DJI Matrice 300 RTK with Zenmuse P1 Camera.*

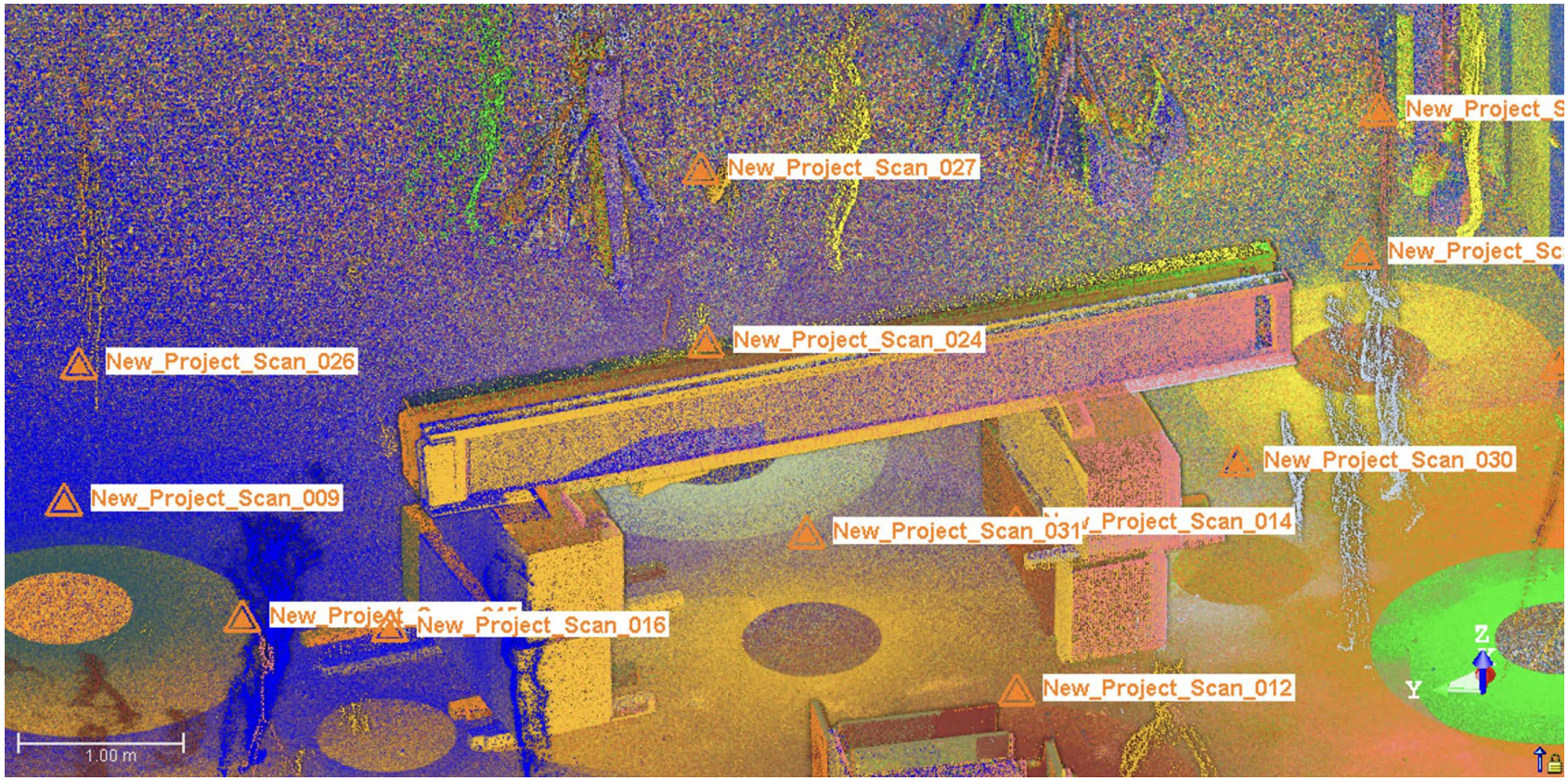

Figure A.3 *Top-Down View of a Registered Terrestrial LiDAR Point Cloud Depicting a Bridge Structure and Surrounding Area.*

Table A.2 *Equipment Lists.*

Item	Quantity	Key Details
DJI Matrice 300 RTK SP Combo	1	Professional drone with maximum flight time of 55 minutes, 15 km transmission range, 6-directional obstacle sensing, IP45 weather resistance rating, triple redundant systems for safety, payload capacity up to 2.7 kg, and RTK positioning system for centimeter-level accuracy. Includes 2 TB60 Intelligent Flight Batteries and BS60 Intelligent Battery Station.
DJI Zenmuse L1	1	Integrated LiDAR, IMU and camera payload featuring Livox LiDAR sensor with 450,000 points per second scanning capability, 2 cm vertical accuracy, 5 cm horizontal accuracy, 3-axis stabilized gimbal, 70° field of view, integrated 20MP RGB camera for simultaneous LiDAR and photogrammetry capture.
DJI Zenmuse P1	1	Full-frame 45MP sensor camera payload with mechanical shutter (1/2000s), 3-axis stabilized gimbal, interchangeable fixed-focus lenses, smart oblique capture capabilities, 3 cm mapping accuracy without GCPs, and time-synchronized positioning data for precise image georeferencing.
DJI Matrice 300 TB60 Intelligent Flight Battery	2	Additional batteries for extended flight time
JZ T90 Spotlight for DJI	1	Accessory light for drone operations
DJI Matrice 300 Upward Gimbal Connector	1	Mount for upward-facing payloads
DJI Avata 2 Drone Fly More Combo	1	Compact FPV drone with 18-minute flight time, 10 km transmission range, 4K/60fps video recording, 48MP photo capture, 155° ultra-wide field of view, built-in propeller guards for safety, forward/downward/backward obstacle sensing, and 20 m/s maximum speed. Combo includes additional accessories, landing pad, and 128GB microSD card.
DJI Avata 2 Intelligent Flight Battery	1	Additional battery for Avata 2 drone
DJI Avata 2 Battery Charging Hub	1	Multi-battery charging station

About the Joint Transportation Research Program (JTRP)

On March 11, 1937, the Indiana Legislature passed an act which authorized the Indiana State Highway Commission to cooperate with and assist Purdue University in developing the best methods of improving and maintaining the highways of the state and the respective counties thereof. That collaborative effort was called the Joint Highway Research Project (JHRP). In 1997 the collaborative venture was renamed as the Joint Transportation Research Program (JTRP) to reflect the state and national efforts to integrate the management and operation of various transportation modes.

The first studies of JHRP were concerned with Test Road No. 1—evaluation of the weathering characteristics of stabilized materials. After World War II, the JHRP program grew substantially and was regularly producing technical reports. Over 1,600 technical reports are now available, published as part of the JHRP and subsequently JTRP collaborative venture between Purdue University and what is now the Indiana Department of Transportation.

Free online access to all reports is provided through a unique collaboration between JTRP and Purdue Libraries. These are available at docs.lib.purdue.edu/jtrp/.

Further information about JTRP and its current research program is available at engineering.purdue.edu/JTRP.

About This Report

An open access version of this publication is available online. See the URL in the citation below.

Kang, K., Xiao, J., Hu, J., Kanakamedala, D. S. C., Seo, J., & Varma, A. (2025). *Feasibility of 3D scanning technology for bridge inspection and management* (Joint Transportation Research Program Publication No. FHWA/IN/JTRP-2025/16). West Lafayette, IN: Purdue University. https://doi.org/10.5703/1288284317880